

Coexistence of Pulsed Radar and Communications: Interference Suppression and Multi-path Combining

Haoyu Zhang, Li Chen, *Senior Member, IEEE*, Yunfei Chen, *Senior Member, IEEE*, Huarui Yin and Guo Wei

Abstract—The focus of this study is on the spectrum sharing between multiple-input multiple-output (MIMO) communications and co-located pulsed MIMO radar systems in multi-path environments. The major challenge is to suppress the mutual interference between the two systems while combining the useful multi-path components received at each system. We tackle this challenge by jointly designing the communication precoder, radar transmit waveform and receive filter. Specifically, the signal-to-interference-plus-noise ratio (SINR) at the radar receiver is maximized subject to constraints on the radar waveform, communication rate and transmit power. The multi-path propagation complicates the expressions of the radar SINR and communication rate, leading to a non-convex problem. To solve it, a sub-optimal algorithm based on the alternating maximization is used to optimize the precoder, radar transmit waveform and receive filter iteratively. The radar receive filter can be updated by a closed-form solution. The communication precoder and radar transmit waveform can be obtained by the successive convex approximation and alternating direction method of multipliers. Simulation results are provided to demonstrate the effectiveness of the proposed design.

Index Terms—MIMO communications, multi-path combining, pulsed radar, radar and communication coexistence.

I. INTRODUCTION

THE explosive growth of mobile devices has placed an urgent demand for exploring extra radio spectrum resources. To cope with that, the frequency bands traditionally occupied by radar systems are shared with the wireless communication systems, e.g., sub-6 GHz band leveraged by air traffic control radars and long-range weather radars [1], and the millimeter wave (mmWave) band conventionally assigned to automotive radars and high-resolution imaging radars [2]. This has led to strong interest in the coexistence of radar and communication (CRC) [3].

The primary challenge of CRC is to manage the mutual interference in a multi-path environment generated by surrounding scatterers. Early studies included policies for opportunistic spectrum access [4], separate radar waveform [5], [6] and communication receiver [7] design. The joint design of the radar and communication signals increases the degrees of cooperation between the two systems, thus suppressing the interference more effectively. The cooperative spectrum sharing between a single-input single-output (SISO) pulsed radar and a SISO communication system was considered in

[8], [9]. Specifically, in [8], the performance metric of the communication system was formulated as a weighted sum of rates with and without the radar interference, which is then maximized with constraints on radar signal-to-interference-plus-noise-ratio (SINR) and transmit power. The work of [9] investigated radar-oriented multi-carrier CRC systems and developed optimum power allocation strategies to maximize the radar SINR subject to communication throughput and power constraints.

For the multiple-input multiple-output (MIMO) CRC systems, multi-path propagation will pose greater challenges to cooperative interference management in the space-time domain [10], [11]. In [10], the communication codebook was jointly designed with MIMO-matrix completion (MC) radar sampling scheme to minimize the effective interference power at a specific resolution cell of the radar system, while the average capacity and transmit power constraints on the communication system were taken into account. The design criterion adopted in [11] was the maximization of mutual information for the MIMO communication system while safeguarding the SINR performance at multiple resolution cells monitored by the radar system. A more practical multiple-antenna scenario was considered in [12], [13], where the radar waveform was chosen to bear the requirements concerning range resolution, sidelobe level and envelope constancy. In [12], the radar SINR at a single resolution cell was maximized subject to the constraints on the transmit power, the communication rate and the similarity of the radar waveform to a reference signal. In [13], the figure of merit was constructed as the inverse of the harmonic mean of the radar SINR across multiple resolution cells, which was minimized under the constraints similar to those in [12].

The existing literature on CRC has only considered the multi-path propagation in the interference between the two systems. However, the desired signals at the receiver in each system also suffer from multi-path in practical scenarios. Specifically, at the radar receiver, the useful target multi-path returns include not only the backscattered signal along line-of-sight (LOS), but also echoes from scatterers. Similarly, at the communication receiver, the useful data signals may contain a direct path component as well as indirect multi-path components. To improve the performance of individual systems, it is necessary to combine these multi-path components in each system. For the pulsed radar system, several studies have demonstrated that multi-path propagation can increase its spatial diversity and further improve its detection performance when the statistical characterization of multi-path returns was known [14]–[17]. For the communication

Haoyu Zhang, Li Chen, Huarui Yin and Guo Wei are with the CAS Key Laboratory of Wireless-Optical Communications, University of Science and Technology of China, Hefei 230027, China (e-mail: hyzhangy@mail.ustc.edu.cn; {chenli87, yhr, wei}@ustc.edu.cn).

Yunfei Chen is with the School of Engineering, University of Warwick, Coventry CV4 7AL, U.K. (e-mail: yunfei.chen@warwick.ac.uk).

system, the combining of multi-path components for better data transmission has also been widely studied [18], [19].

However, these techniques cannot be directly applied to the CRC systems due to the coupled communication and radar performance. Specifically, the signals from the communication system are the interference to the radar receiver and vice versa, which leads to the conflict of their performances. Since existing multi-path combining techniques are developed for individual systems, they cannot manage mutual interference and are not suitable for coexistence. To the best of our knowledge, combining useful multi-path signals from individual systems and simultaneously suppressing the mutual interference between the two systems for better detection performance and higher data rates has not been investigated before.

Motivated by the above observations, in this work, we jointly design the communication precoder, radar transmit waveform and receive filter for efficient coexistence between a co-located pulsed MIMO radar and a single-user MIMO communication system in multi-path environments. The SINR is taken as the performance metric of the radar system. In order to effectively utilize the diversity gain brought by multi-path propagation, the multi-path channel between the radar and the target is assumed known, so that the multi-path returns of the target can be exploited to further improve the SINR. For the communication system, the transmission rate is considered, where the multi-path components are also known. The existence of the mutual interference makes the simultaneous optimization of the SINR and rate difficult. In order to mitigate the impact of interference on the considered CRC system, we formulate the radar-centric design strategy, where the radar SINR is maximized with constraint on the communication transmission rate. The resulting problem is complex due to the non-convex constraints and non-concave objective function. We propose an iterative algorithm to solve it with low complexity. The main contributions are summarized as follows.

- For pulsed CRC systems, multi-path exists in both radar detection and communication data transmission. Different from previous works, we consider not only interference suppression in multi-path environments, but also multi-path combining. To achieve this, we develop a joint design of the communication precoder, radar transmit waveform and receive filter. The resulting optimization problem is a fractional programming with non-convex constraints.
- Since the formulated problem is non-convex, we first adopt the alternating optimization method to decouple the optimization variables. Then, the closed form of the receive filter is derived analytically, and the non-convexity of the sub-problems about the communication precoder and radar waveform are tackled by the successive convex approximation (SCA), where each convex approximation problem is solved by the interior-point method.
- Since the interior-point method will give rise to high complexity, we utilize the alternating direction method of multipliers (ADMM) to accelerate the solution of each convex approximation problem in the SCA procedure. We

also consider some common radar waveform constraints (e.g., the similarity, per-antenna power and the peak-to-average power ratio (PAPR) constraints) and extend the proposed waveform design to these more practical scenes.

The remainder of the paper is organized as follows. Section II introduces the system model and formulates the optimization problem. The SCA-based algorithm for obtaining the communication precoder is presented in Section III. Section IV develops effective radar waveform design algorithms for the multi-path combining and multi-path suppression scenarios, respectively. The numerical results are given in Section V, followed by the conclusions drawn in Section VI.

Notations: We use bold lowercase letters to represent column vectors, and bold uppercase letters to represent matrices. The operators $(\cdot)^T$, $(\cdot)^*$ and $(\cdot)^H$ correspond to the transpose, conjugate and Hermitian transpose, respectively. $\text{tr}(\mathbf{A})$, $|\mathbf{A}|$, $\text{rank}(\mathbf{A})$ and $\text{vec}(\mathbf{A})$ stand for the trace, the determinant, the rank and the vectorization operation of the matrix \mathbf{A} , respectively. $\mathcal{M}(\mathbf{A})$ denotes the normalized principle eigenvector of \mathbf{A} . $\mathbf{A} \succ \mathbf{0}$ ($\mathbf{A} \succeq \mathbf{0}$) indicates that \mathbf{A} is positive definite (positive semidefinite). $\|\mathbf{a}\|$ is the Euclidean norm of the vector \mathbf{a} . \mathbf{I}_M is a $M \times M$ identity matrix. The symbol \otimes represents the Kronecker product. $\mathbb{C}^{M \times N}$ denotes the set of complex-valued $M \times N$ matrices. $\Re\{x\}$ refers to the real parts of a complex number x . $\mathbb{E}(\cdot)$ denotes the statistical expectation. Finally, $\mathbf{x} \sim \mathcal{CN}(\mathbf{a}, \mathbf{A})$ means that \mathbf{x} follows a complex Gaussian distribution with mean \mathbf{a} and covariance matrix \mathbf{A} .

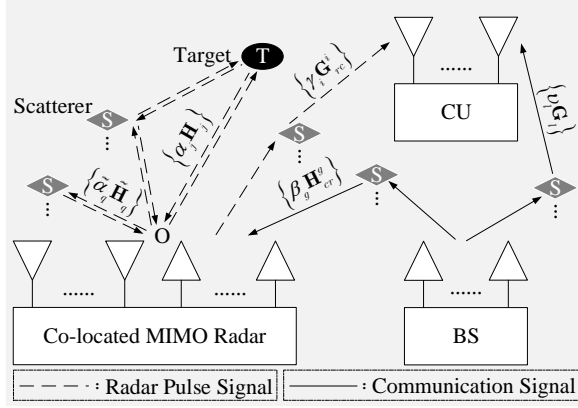
II. SYSTEM MODEL AND PROBLEM FORMULATION

We consider the scenario illustrated in Fig. 1a, where a co-located pulsed MIMO radar operates on the same frequency band as a single-user MIMO communication system. The communication system is composed of a base station (BS) and a communication user (CU) equipped with N_T and N_R antennas, respectively, where the BS serves the CU with desired rates in the presence of multi-path propagation generated by far-field scatterers. The radar system is equipped with M_T transmit and M_R receive antennas with the goal of detecting a point-like target located within the coverage of the BS. All antennas are assumed to be deployed in half-wavelength spaced uniform linear arrays.

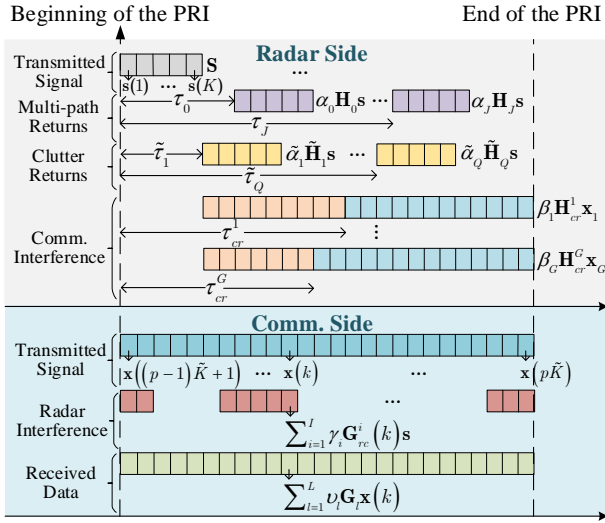
As depicted in Fig. 1b, the radar pulse signal is transmitted at a duration of K/B , where B denotes the sampling rate of the radar system. A burst of P pulses are transmitted at a pulse repetition interval (PRI) of \tilde{K}/B in a coherent processing interval (CPI), and P is chosen in such a way that no cell migration takes place in the CPI [8]. Denote $\mathbf{s}(k) \in \mathbb{C}^{M_T \times 1}$ as the discrete-time transmitted signal at time instant k for $(k \bmod \tilde{K}) \in \{1, \dots, \tilde{K}\}$. Then, the transmit radar waveform during each PRI can be represented by $\mathbf{S} = [\mathbf{s}(1) \cdots \mathbf{s}(\tilde{K})] \in \mathbb{C}^{M_T \times \tilde{K}}$.

For the communication system, the BS continuously transmits communication symbols to the CU during the CPI¹. The

¹The communication system is assumed to share the same sampling rate as the radar system and achieve the synchronizations of the sampling time [20]. A total of P frames are transmitted in the scheduling window with the frame duration equal to the radar PRI \tilde{K}/B .



(a) Spectrum sharing between a co-located MIMO radar and a MIMO communication system in multi-path environments.



(b) Transmitted and received signals of each system in the p -th PRI.

Fig. 1. System model of pulsed CRC.

symbol vector transmitted at time instant k is denoted by $\mathbf{d}(k) \in \mathbb{C}^{D \times 1}$ with D being the number of data streams and satisfying $D \leq \min\{N_T, N_R\}$. These symbols are assumed to be independent and identically Gaussian distributed, i.e., $\mathbf{d}(k) \sim \mathcal{CN}(\mathbf{0}, \mathbf{I}_D), \forall k$. Denote the precoder for the BS as $\mathbf{V} \in \mathbb{C}^{N_T \times D}$. After precoder, the symbol vectors for the CU become $\mathbf{x}(k) = \mathbf{V}\mathbf{d}(k) \in \mathbb{C}^{N_T \times 1}, \forall k$.

A. Radar Performance

Assume that the target is located at a range of R from the radar in the angular direction of θ_0 , where R satisfies $K/B \leq 2R/c \leq (K-K)/B$ with c denoting the speed of light. Therefore, the target will be present in an unknown range cell τ_0 with $\tau_0 \in \{K, \dots, \hat{K} - K\}$, i.e., the radar pulse hits the target with a round-trip delay τ_0/B . To simplify the exposition and without loss of generality, we analyze the received signals in the p -th PRI. As shown in Fig. 1, the radar multi-path signals reflected off the target consist of a

direct path and several indirect returns, which are overlaid with clutter returns, communication interference and noise. The communication interference is persistent throughout the time period $[(p-1)\hat{K} + K, p\hat{K}]$, and the multi-path and clutter returns may be distributed in different range cells. Denoting $\hat{K} = \hat{K} - K$, the received space-time signal $\mathbf{Y} \in \mathbb{C}^{M_R \times \hat{K}}$ can be modeled as

$$\mathbf{Y} = \mathbf{Y}_m + \mathbf{Y}_s + \mathbf{Y}_{cr} + \mathbf{Y}_n, \quad (1)$$

where \mathbf{Y}_m denotes the multi-path returns of the target; \mathbf{Y}_s denotes the clutter return; \mathbf{Y}_{cr} denotes the communication interference and \mathbf{Y}_n denotes the additive noise. The entries of \mathbf{Y}_n are modeled as independent complex Gaussian random variables with zero mean and variance σ_r^2 .

Suppose that there exists J uncorrelated scatterers causing the indirect path target returns, where the j -th scatterer has an angle of θ_j to the radar receiver and its corresponding indirect paths have a propagation delay of τ_j . Note that each scatterer will result in two types of indirect path returns (see $\overrightarrow{OS} \rightarrow \overrightarrow{ST} \rightarrow \overrightarrow{TO}$ and $\overrightarrow{OT} \rightarrow \overrightarrow{TS} \rightarrow \overrightarrow{SO}$ in Fig. 1a). Then, \mathbf{Y}_m can be formulated as²

$$\mathbf{Y}_m = \alpha_0 \mathbf{v}_r(\theta_0) \mathbf{v}_t^T(\theta_0) \mathbf{SD}(\tau_0) + \sum_{j=1}^J \alpha_j [\mathbf{v}_r(\theta_0) \mathbf{v}_t^T(\theta_j) + \mathbf{v}_r(\theta_j) \mathbf{v}_t^T(\theta_0)] \mathbf{SD}(\tau_j), \quad (2)$$

where $\alpha_j = \alpha_0 \rho_j$ with α_0 and $\rho_j \sim \mathcal{CN}(0, \sigma_{\rho_j}^2)$ denoting the complex amplitude of the target and the j -th scatterer, respectively; $\mathbf{v}_t(\theta)$ and $\mathbf{v}_r(\theta)$ denote the transmit steering vector and receive steering vector of the radar at angle θ , respectively, given by

$$\mathbf{v}_t(\theta) = \frac{1}{\sqrt{M_T}} [1, e^{-j\pi \sin \theta}, \dots, e^{-j\pi(M_T-1) \sin \theta}]^T,$$

$$\mathbf{v}_r(\theta) = \frac{1}{\sqrt{M_R}} [1, e^{-j\pi \sin \theta}, \dots, e^{-j\pi(M_R-1) \sin \theta}]^T;$$

and $\mathbf{D}(\tau) = [\mathbf{0}_{K \times (\tau-K)} \quad \mathbf{I}_K \quad \mathbf{0}_{K \times (\hat{K}-\tau)}] \in \mathbb{C}^{K \times \hat{K}}$ denotes the time delayed matrix.

Assume the presence of Q scatterers causing clutter returns with the q -th scatterer located at the range cell $\tilde{\tau}_q$ in the angular direction of $\tilde{\theta}_q$. Then, \mathbf{Y}_s is given by

$$\mathbf{Y}_s = \sum_{q=1}^Q \tilde{\alpha}_q \mathbf{v}_r(\tilde{\theta}_q) \mathbf{v}_t^T(\tilde{\theta}_q) \mathbf{SD}(\tilde{\tau}_q), \quad (3)$$

where $\tilde{\alpha}_q \sim \mathcal{CN}(0, \sigma_{\tilde{\alpha}_q}^2)$ accounts for the complex scattering coefficient of the q -th scatterer in clutter.

We also consider G -path channels between the BS and the radar receiver. Denote the direction of departure (DoD), direction of arrival (DoA) and delay of the g -th path by φ_{cr}^g , ϕ_{cr}^g and τ_{cr}^g , respectively. Then, \mathbf{Y}_{cr} can be modeled by

$$\mathbf{Y}_{cr} = \sum_{g=1}^G \beta_g \mathbf{v}_r(\phi_{cr}^g) \mathbf{a}_t^T(\varphi_{cr}^g) \mathbf{X}_g, \quad (4)$$

²Possible Doppler phase variations can be ignored within a PRI, since one single PRI duration \hat{K}/B is generally short [11].

where $\beta_g \sim \mathcal{CN}(0, \sigma_{\beta,g}^2)$ is the gain of the g -th path; $\mathbf{a}_t(\varphi)$ denotes the transmit steering vector of the BS at angle φ , given by

$$\mathbf{a}_t(\varphi) = \frac{1}{\sqrt{N_T}} \left[1, e^{-j\pi \sin \varphi}, \dots, e^{-j\pi(N_T-1) \sin \varphi} \right]^T;$$

and $\mathbf{X}_g = \left[\mathbf{x} \left(K - \tau_{cr}^g + (p-1)\tilde{K} + 1 \right) \cdots \mathbf{x} \left(p\tilde{K} - \tau_{cr}^g \right) \right]$ denotes the communication data segment received by the radar in the p -th PRI.

Finally, we can recast \mathbf{Y} in vector form as

$$\mathbf{y} = \sum_{j=0}^J \alpha_j \mathbf{H}_j \mathbf{s} + \sum_{q=1}^Q \tilde{\alpha}_q \tilde{\mathbf{H}}_q \mathbf{s} + \sum_{g=1}^G \beta_g \mathbf{H}_{cr}^g \mathbf{x}_g + \mathbf{y}_n, \quad (5)$$

where $\mathbf{H}_0 = \mathbf{D}^T(\tau_0) \otimes (\mathbf{v}_r(\theta_0) \mathbf{v}_t^T(\theta_0))$; $\mathbf{H}_j = \mathbf{D}^T(\tau_j) \otimes (\mathbf{v}_r(\theta_0) \mathbf{v}_t^T(\theta_j) + \mathbf{v}_r(\theta_j) \mathbf{v}_t^T(\theta_0))$; $\tilde{\mathbf{H}}_q = \mathbf{D}^T(\tilde{\tau}_q) \otimes (\mathbf{v}_r(\tilde{\theta}_q) \mathbf{v}_t^T(\tilde{\theta}_q))$; $\mathbf{H}_{cr}^g = \mathbf{I}_{\tilde{K}} \otimes \mathbf{v}_r(\phi_{cr}^g) \mathbf{a}_t^T(\varphi_{cr}^g)$; $\mathbf{s} = \text{vec}(\mathbf{S})$, $\mathbf{x}_g = \text{vec}(\mathbf{X}_g)$ and $\mathbf{y}_n = \text{vec}(\mathbf{Y}_n)$.

In order to achieve the best detection performance, we combine the multi-path returns to maximize the output SINR³. After \mathbf{y} being filtered by a space-time filter $\mathbf{w} \in \mathbb{C}^{M_R \tilde{K}}$, the SINR can be constructed as (6), as shown at the top of next page, where $\sigma_{\alpha,0}^2 = |\alpha_0|^2$ and $\sigma_{\alpha,j}^2 = |\alpha_0|^2 \sigma_{\rho,j}^2$, $j = 1, \dots, J$ and

$$\begin{aligned} \mathbf{R}(\mathbf{V}, \mathbf{s}) &= \sum_{g=1}^G \sigma_{\beta,g}^2 \mathbf{H}_{cr}^g (\mathbf{I}_{\tilde{K}} \otimes \mathbf{V} \mathbf{V}^H) (\mathbf{H}_{cr}^g)^H \\ &+ \sum_{q=1}^Q \sigma_{\tilde{\alpha},q}^2 \tilde{\mathbf{H}}_q \mathbf{s} \mathbf{s}^H \tilde{\mathbf{H}}_q^H + \sigma_r^2 \mathbf{I}_{M_R \tilde{K}}. \end{aligned} \quad (7)$$

It can be observed from (6) that the optimal \mathbf{w} for the space-time filter can be obtained by maximizing the generalized Rayleigh quotient of $\Psi(\mathbf{s}) = \sum_{j=0}^J \sigma_{\alpha,j}^2 \mathbf{H}_j \mathbf{s} \mathbf{s}^H \mathbf{H}_j^H$ and $\mathbf{R}(\mathbf{V}, \mathbf{s})$, i.e.,

$$\mathbf{w}^* = \arg \max_{\mathbf{w}} \frac{\mathbf{w}^H \Psi(\mathbf{s}) \mathbf{w}}{\mathbf{w}^H \mathbf{R}(\mathbf{V}, \mathbf{s}) \mathbf{w}} = \mathcal{M}(\mathbf{R}^{-1}(\mathbf{V}, \mathbf{s}) \Psi(\mathbf{s})). \quad (8)$$

Then, using (8), SINR($\mathbf{w}, \mathbf{s}, \mathbf{V}$) can be reformulated as

$$\text{SINR}(\mathbf{s}, \mathbf{V}) = \sum_{j=0}^J \sigma_{\alpha,j}^2 \frac{\mathbf{s}^H \mathbf{H}_j \mathbf{H}_j^H \mathbf{w} \mathbf{w}^H \mathbf{H}_j \mathbf{s}}{\mathbf{s}^H \tilde{\mathbf{R}} \mathbf{s} + r(\mathbf{V})}, \quad (9)$$

where $r(\mathbf{V}) = \mathbf{w}^H \left(\sum_{g=1}^G \sigma_{\beta,g}^2 \mathbf{H}_{cr}^g (\mathbf{I}_{\tilde{K}} \otimes \mathbf{V} \mathbf{V}^H) (\mathbf{H}_{cr}^g)^H + \sigma_r^2 \mathbf{I}_{M_R \tilde{K}} \right) \mathbf{w}$ and $\tilde{\mathbf{R}} = \sum_{q=1}^Q \sigma_{\tilde{\alpha},q}^2 \tilde{\mathbf{H}}_q^H \mathbf{w} \mathbf{w}^H \tilde{\mathbf{H}}_q$.

We assume that θ_0 can be obtained from DOA estimation methods [22] and α_0 can be estimated by the Angle and Phase Estimation (APES) algorithm [23]. $\{\theta_j, \sigma_{\rho,j}^2\}_{j=1}^J$, $\{\tilde{\theta}_q, \sigma_{\tilde{\alpha},q}^2\}_{q=1}^Q$ and $\{\varphi_{cr}^g, \phi_{cr}^g, \sigma_{\beta,g}^2\}_{g=1}^G$ can be acquired by some cognitive methods or from some historical data [24], [25]. Also, we assume that these parameters remain unchanged in a CPI.

³The detection probability monotonically increases with respect to (w.r.t.) the output SINR under Gaussian conditions [21].

B. Communication Performance

The signal received by the CU in the p -th PRI is also shown in Fig. 1b, which is subject to intermittent radar interference and noise. Then, the received signal at time instant k can be modeled by

$$\mathbf{r}(k) = \mathbf{r}_m(k) + \mathbf{r}_{rc}(k) + \mathbf{r}_n(k), \quad (10)$$

where $\mathbf{r}_m(k)$ denotes the desired communication signal, $\mathbf{r}_{rc}(k)$ denotes the radar interference and $\mathbf{r}_n(k)$ denotes the additive noise. The entries of $\mathbf{r}_n(k)$ are independent complex Gaussian random variables with zero mean and variance σ_c^2 .

Denote L as the number of paths between the BS and the CU. The DoD and DoA of the l -th path are represented by ϑ_t^l and ϑ_r^l , respectively. Since the delay of each path will distort the received communication symbols at the CU, we assume that the effect can be perfectly pre-compensated at the BS with given estimated delay parameters by using existing compensation methods [18], [19]. Then, $\mathbf{r}_m(k)$ can be formulated as

$$\mathbf{r}_m(k) = \sum_{l=1}^L v_l \mathbf{G}_l \mathbf{x}(k), \quad (11)$$

where $v_l \sim \mathcal{CN}(0, \sigma_{v,l}^2)$ and $\mathbf{G}_l = \mathbf{a}_r(\vartheta_r^l) \mathbf{a}_t^T(\vartheta_t^l)$ denote the gain and the transmit-receive steering matrix of the l -th path, respectively, while $\mathbf{a}_r(\vartheta)$ is the receive steering vector of the CU at angle ϑ , given by

$$\mathbf{a}_r(\vartheta) = \frac{1}{\sqrt{N_R}} \left[1, e^{-j\pi \sin \vartheta}, \dots, e^{-j\pi(N_R-1) \sin \vartheta} \right]^T.$$

Note that the communication multi-path channel is equivalent to a bi-static radar channel [26], which is different from the radar channel in the mono-static case of (2).

Assuming I scatterers reflecting the radar pulses towards the CU, $\mathbf{r}_{rc}(k)$ can be expressed as

$$\mathbf{r}_{rc}(k) = \sum_{i=1}^I \gamma_i \mathbf{a}_r(\varphi_{rc}^i) \mathbf{v}_t^T(\phi_{rc}^i) \mathbf{s}(k - \tau_{rc}^i), \quad (12)$$

where $\gamma_i \sim \mathcal{CN}(0, \sigma_{\gamma,i}^2)$ accounts for the gain of the i -th scattering path; φ_{rc}^i , ϕ_{rc}^i and $\tau_{rc}^i \in \{0, \dots, \tilde{K} - 1\}$ are the DoA, DoD and the delay of the i -th path, respectively. The intermittent nature of the radar interference can be characterized by the following matrix \mathbf{L}_i ,

$$\mathbf{L}_i = \begin{cases} [\mathbf{0}_{K, \tau_{rc}^i} & \mathbf{I}_K & \mathbf{0}_{K, \tilde{K} - K - \tau_{rc}^i}], & \text{if } \tau_{rc}^i \in \mathcal{K}1 \\ [\mathbf{J}_{\tilde{K} - \tau_{rc}^i} & \mathbf{0}_{K, \tilde{K} - 2K} & \mathbf{J}_{-K + \tilde{K} - \tau_{rc}^i}], & \text{if } \tau_{rc}^i \in \mathcal{K}2 \end{cases}$$

where $\mathcal{K}1 = \{0, \dots, \tilde{K} - K\}$, $\mathcal{K}2 = \{\tilde{K} - K + 1, \dots, \tilde{K} - 1\}$ and $\mathbf{J}_k \in \mathbb{C}^{K \times \tilde{K}}$ is the shift matrix with

$$\mathbf{J}_k(i, j) = \begin{cases} 1, & \text{if } i - j = k \\ 0, & \text{if } i - j \neq k \end{cases}$$

Then, we have $\mathbf{s}(k - \tau_{rc}^i) = \mathbf{S} \mathbf{L}_i \mathbf{e}(k - (p-1)\tilde{K}) = \left(\mathbf{e}^T(k - (p-1)\tilde{K}) \mathbf{L}_i^T \otimes \mathbf{I}_{M_T} \right) \mathbf{s}$, where $\mathbf{e}(n) \in \mathbb{C}^{\tilde{K}}$ is a direction vector whose n -th entry is one, while all the other

$$\text{SINR}(\mathbf{w}, \mathbf{s}, \mathbf{V}) = \frac{\mathbb{E} \left\{ \left| \mathbf{w}^H \sum_{j=0}^J \alpha_j \mathbf{H}_j \mathbf{s} \right|^2 \right\}}{\mathbb{E} \left\{ \left| \mathbf{w}^H \sum_{q=1}^Q \tilde{\alpha}_q \tilde{\mathbf{H}}_q \mathbf{s} \right|^2 \right\} + \mathbb{E} \left\{ \left| \mathbf{w}^H \sum_{g=1}^G \beta_g \mathbf{H}_{cr}^g \mathbf{x}_g \right|^2 \right\} + \sigma_r^2 \mathbf{w}^H \mathbf{w}} = \sum_{j=0}^J \sigma_{\alpha,j}^2 \frac{\mathbf{w}^H \mathbf{H}_j \mathbf{s} \mathbf{s}^H \mathbf{H}_j^H \mathbf{w}}{\mathbf{w}^H \mathbf{R}(\mathbf{V}, \mathbf{s}) \mathbf{w}}. \quad (6)$$

entries equal to zero. Thus, the radar interference $\mathbf{r}_{rc}(k)$ can be rewritten as

$$\mathbf{r}_{rc}(k) = \sum_{i=1}^I \gamma_i \mathbf{G}_{rc}^i(k) \mathbf{s}, \quad (13)$$

where $\mathbf{G}_{rc}^i(k) = \mathbf{a}_r(\varphi_{rc}^i) \mathbf{v}_t^T(\phi_{rc}^i) (\mathbf{e}^T(k - (p-1)\tilde{K}) \tilde{\mathbf{L}}_i^T \otimes \mathbf{I}_{M_T})$.

Using (10), (11) and (13), the achievable transmission rate at time instant k can be calculated as

$$\text{MI}_k(\mathbf{s}, \mathbf{V}) = \log \left| \left(\sum_{l=1}^L \sigma_{v,l}^2 \mathbf{G}_l \mathbf{V} \mathbf{V}^H \mathbf{G}_l^H \right) (\mathbf{R}_c^k(\mathbf{s}))^{-1} + \mathbf{I}_{N_R} \right|, \quad (14)$$

where $\mathbf{R}_c^k(\mathbf{s}) = \sigma_c^2 \mathbf{I}_{N_R} + \sum_{i=1}^I \sigma_{\gamma,i}^2 \mathbf{G}_{rc}^i(k) \mathbf{s} \mathbf{s}^H (\mathbf{G}_{rc}^i(k))^H$. Then, the average communication rate during the p -th PRI is given by

$$\text{MI}(\mathbf{s}, \mathbf{V}) = \frac{1}{\tilde{K}} \sum_{k=1}^{\tilde{K}} \text{MI}_k(\mathbf{s}, \mathbf{V}). \quad (15)$$

Similar to the radar system, we also assume that $\{\mathbf{G}_l, \sigma_{v,l}^2\}_{l=1}^L$ and $\{\varphi_{rc}^i, \phi_{rc}^i, \sigma_{\gamma,i}^2\}_{i=1}^I$ can be estimated and remain unchanged in a CPI.

C. Problem Formulation

For the radar system, the relevant figure of merit is the output SINR defined in (9). For the communication system, the relevant merit is the transmission rate given by (15). Tradeoff is required due to the existence of the mutual interference. To effectively suppress it, we jointly design the radar waveform \mathbf{s} and the communication precoder \mathbf{V} to maximize the radar SINR while guaranteeing a minimum required communication transmission rate, denoted by MI_0 . The corresponding optimization problem is formulated as follows.

$$\mathcal{P}0: \max_{\mathbf{s}, \mathbf{V}} \sum_{j=0}^J \sigma_{\alpha,j}^2 \frac{\mathbf{s}^H \mathbf{H}_j^H \mathbf{w} \mathbf{w}^H \mathbf{H}_j \mathbf{s}}{\mathbf{s}^H \tilde{\mathbf{R}} \mathbf{s} + r(\mathbf{V})} \quad (16a)$$

$$\text{s.t. } \text{MI}(\mathbf{s}, \mathbf{V}) \geq \text{MI}_0 \quad (16a)$$

$$\text{tr}(\mathbf{V} \mathbf{V}^H) \leq P_B \quad (16b)$$

$$\|\mathbf{s}\|^2 \leq P_R, \quad (16c)$$

where P_B and P_R denote the maximum transmit power of the BS and the radar, respectively.

$\mathcal{P}0$ is NP-hard due to the non-concave objective function and non-convex constraint (16a). The coupling of \mathbf{V} and \mathbf{s} makes it difficult. We can adopt the alternating optimization method to optimize \mathbf{V} and \mathbf{s} iteratively, which has been widely applied in the coexistence of radar and communication [11],

[12], [20]. Specifically, we will decompose $\mathcal{P}0$ into two sub-problems for \mathbf{V} and \mathbf{s} , respectively. Multi-path propagation becomes a challenge to solving each sub-problem. We will then develop fast algorithms with a polynomial computational complexity to get high-quality solutions.

III. COMMUNICATION PRECODER DESIGN

In this section, we will consider the optimization of the communication precoder \mathbf{V} with fixed radar waveform \mathbf{s} , that is,

$$\mathcal{P}1: \min_{\mathbf{V}} r(\mathbf{V}) \quad (17)$$

$$\text{s.t. } (16a), (16b).$$

$\mathcal{P}1$ is challenging due to the non-convex constraint (16a). Multi-path propagation and the dynamic interference make it difficult to deal with this non-convexity. Note that the precoding design proposed in [10] can effectively match the variation of interference and achieves adaptive data transmission. However, it is not suitable for the multi-path scenario considered here. Moreover, the high complexity of designing and implementing the precoders for each communication symbol also limits its use. In the following, we will obtain a general precoder for each frame by solving $\mathcal{P}1$ with the SCA and ADMM, which will greatly reduce complexity compared with the adaptive precoding design in [10].

A. Sub-Optimal Solution Based on SCA

This subsection focuses on approximating $\mathcal{P}1$ by a series of convex quadratically constrained quadratic programming (QCQP) problems. We first need to construct a surrogate function to approximate $\text{MI}(\mathbf{s}, \mathbf{V})$ defined in (15), so that the SCA method can be used to eliminate the non-convexity of (16a). Since $\text{MI}(\mathbf{s}, \mathbf{V})$ is non-convex w.r.t. \mathbf{V} , it is challenging to derive its minorizer using the first-order Taylor expansion. To proceed, we resort to the following lemma to convert $\text{MI}(\mathbf{s}, \mathbf{V})$ to a tractable form.

Lemma 1 (Transformation of $\text{MI}(\mathbf{s}, \mathbf{V})$): $\text{MI}(\mathbf{s}, \mathbf{V})$ can be equivalently rewritten as

$$\text{MI}(\mathbf{v}) = \frac{1}{\tilde{K}} \sum_{k=1}^{\tilde{K}} \log \left| \mathbf{C}(\mathbf{E}_k(\mathbf{v}))^{-1} \mathbf{C}^H \right|, \quad (18)$$

where $\mathbf{v} = \text{vec}(\mathbf{V})$, $\mathbf{C} = [\mathbf{I}_{N_R N_T D}, \mathbf{0}_{N_R N_T D \times N_R}]$ and

$$\mathbf{E}_k(\mathbf{v}) = \begin{bmatrix} \mathbf{I}_{N_R N_T D} & \Delta^{\frac{1}{2}} (\mathbf{I}_{N_R} \otimes \mathbf{v}^*) \\ (\mathbf{I}_{N_R} \otimes \mathbf{v}^T) \Delta^{\frac{1}{2}} & \mathbf{R}_c^k(\mathbf{s}) + (\mathbf{I}_{N_R} \otimes \mathbf{v}^T) \Delta (\mathbf{I}_{N_R} \otimes \mathbf{v}^*) \end{bmatrix}. \quad (19)$$

with Δ defined in (65).

Proof: See Appendix A. ■

Note that $\text{MI}(\mathbf{v})$ is convex w.r.t. $\mathbf{E}_k(\mathbf{v})$ [27]. Then, we can use its first-order condition to approximate (16a) by a series of convex constraints given as follows.

Lemma 2 (SCA-Based Transformation of Constraint (16a)): (16a) can be successively approximated by the following convex quadratic constraint

$$\mathbf{v}^H \bar{\Gamma}_{22}(\bar{\mathbf{v}}) \mathbf{v} - 2\mathcal{R}(\bar{\Gamma}_{12}(\bar{\mathbf{v}}) \mathbf{v}) \leq -\bar{\text{MI}}(\bar{\mathbf{v}}), \quad (20)$$

where $\bar{\Gamma}_{22}(\bar{\mathbf{v}})$, $\bar{\Gamma}_{12}(\bar{\mathbf{v}})$ and $\bar{\text{MI}}(\bar{\mathbf{v}})$ are defined in (75), (76) and (72), respectively, with $\bar{\mathbf{v}}$ being the solution in the previous SCA iteration.

Proof: See Appendix B. ■

Similar to constraint (20), we also need to convert the objective function $r(\mathbf{V})$ into a convex one w.r.t. \mathbf{v} . Before doing so, we first define $\mathbf{W} = \mathbf{w}\mathbf{w}^H$ and partition it into a block matrix, i.e., $\mathbf{W} = (\mathbf{W}_{ij})_{\hat{K} \times \hat{K}}$, where $\mathbf{W}_{ij} \in \mathbb{C}^{M_R \times M_R}$ can be calculated by $\mathbf{W}_{ij} = \mathbf{w}((i-1)M_R + 1 : iM_R) \mathbf{w}^H((j-1)M_R + 1 : jM_R)$ for $(i, j) \in \{1, \dots, \hat{K}\}^2$. Then, $r(\mathbf{V})$ can be transformed to a convex quadratic function in the following lemma.

Lemma 3 (Transformation of $r(\mathbf{V})$): $r(\mathbf{V})$ can be equivalently rewritten as

$$\tilde{r}(\mathbf{v}) = \mathbf{v}^H \mathbf{\Pi} \mathbf{v}, \quad (21)$$

where $\mathbf{\Pi}$ is given by

$$\mathbf{\Pi} = \mathbf{I}_D \otimes \left(\sum_{g=1}^G \sum_{i=1}^{\hat{K}} \sigma_{\beta, g}^2 (\mathbf{T}_{cr}^g)^H \mathbf{W}_{ii} \mathbf{T}_{cr}^g \right) \quad (22)$$

with $\mathbf{T}_{cr}^g = \mathbf{v}_r(\phi_{cr}^g) \mathbf{a}_t^T(\varphi_{cr}^g)$.

Proof: We have

$$\begin{aligned} r(\mathbf{V}) &= \mathbf{w}^H \left(\sum_{g=1}^G \sigma_{\beta, g}^2 \mathbf{H}_{cr}^g (\mathbf{I}_{\hat{K}} \otimes \mathbf{V}\mathbf{V}^H) (\mathbf{H}_{cr}^g)^H \right) \mathbf{w} \\ &\stackrel{(a)}{=} \mathbf{w}^H \left(\sum_{g=1}^G \sigma_{\beta, g}^2 \mathbf{I}_{\hat{K}} \otimes (\mathbf{T}_{cr}^g \mathbf{V}\mathbf{V}^H (\mathbf{T}_{cr}^g)^H) \right) \mathbf{w} \\ &= \sum_{g=1}^G \sigma_{\beta, g}^2 \text{tr} \left((\mathbf{I}_{\hat{K}} \otimes (\mathbf{T}_{cr}^g \mathbf{V}\mathbf{V}^H (\mathbf{T}_{cr}^g)^H)) \mathbf{W} \right) \\ &= \sum_{g=1}^G \sigma_{\beta, g}^2 \sum_{i=1}^{\hat{K}} \text{tr} \left(\mathbf{T}_{cr}^g \mathbf{V}\mathbf{V}^H (\mathbf{T}_{cr}^g)^H \mathbf{W}_{ii} \right) \\ &= \text{tr} \left(\mathbf{V}\mathbf{V}^H \left(\sum_{g=1}^G \sum_{i=1}^{\hat{K}} \sigma_{\beta, g}^2 (\mathbf{T}_{cr}^g)^H \mathbf{W}_{ii} \mathbf{T}_{cr}^g \right) \right) \\ &\stackrel{(b)}{=} \mathbf{v}^H \mathbf{\Pi} \mathbf{v}, \end{aligned} \quad (23)$$

where the procedure (a) comes from $\mathbf{H}_{cr}^g = \mathbf{I}_{\hat{K}} \otimes \mathbf{v}_r(\phi_{cr}^g) \mathbf{a}_t^T(\varphi_{cr}^g)$ and the procedure (b) uses the identity that $\text{tr}(\mathbf{A}_1 \mathbf{A}_2 \mathbf{A}_3 \mathbf{A}_4) = \text{vec}^T(\mathbf{A}_4) (\mathbf{A}_1 \otimes \mathbf{A}_3^T) \text{vec}(\mathbf{A}_2^T)$. It is easy to verify that $\mathbf{\Pi}$ is Hermitian positive semidefinite. ■

Combining the above lemmas, we have the following proposition.

Proposition 1 (SCA-Based Transformation of $\mathcal{P}1$): $\mathcal{P}1$ can be successively approximated by the following QCQP problem

$$\begin{aligned} \mathcal{P}1.1(\bar{\mathbf{v}}): \quad & \min_{\mathbf{v}} \mathbf{v}^H \mathbf{\Pi} \mathbf{v} \\ \text{s.t.} \quad & (20) \\ & \mathbf{v}^H \mathbf{v} \leq P_B. \end{aligned} \quad (24)$$

Denoting the s -th solution of the SCA procedure as $\mathbf{v}^{(s)}$, we can obtain $\mathbf{v}^{(s+1)}$ by solving $\mathcal{P}1.1(\mathbf{v}^{(s)})$.

Proof: With Lemma 3, we give a convex quadratic representation of original objective function $r(\mathbf{V})$. By applying Lemma 1 and Lemma 2, we convert the non-convex constraint (16a) into a convex one. By using the identity that $\text{tr}(\mathbf{A}_1^H \mathbf{A}_2) = \text{vec}^H(\mathbf{A}_1) \text{vec}(\mathbf{A}_2)$, we convert the constraint (16b) to $\mathbf{v}^H \mathbf{v} \leq P_B$. Thus, $\mathcal{P}1.1(\bar{\mathbf{v}})$ is a convex QCQP problem. ■

$\mathcal{P}1.1(\bar{\mathbf{v}})$ can be cast as a second-order cone programming (SOCP) problem and solved by the interior-point methods [28]. Solving the SOCP problem requires $\mathcal{O}(2 \log(1/\varepsilon))$ iterations to converge, where ε denotes the relative accuracy and each iteration has a computational complexity of $\mathcal{O}((DN_T)^3 + DN_T((DN_T)^2 + (DN_T + 1)^2))$ [29]. Denote N_{s1} as the number of iterations for the SCA method. Then, the total complexity of solving $\mathcal{P}1$ using the interior point method and SCA is $\mathcal{O}(2N_{s1}((DN_T)^3 + DN_T((DN_T)^2 + (DN_T + 1)^2)) \log(1/\varepsilon))$. Since the interior-point methods will increase the computation burden in large-scale MIMO systems, we will leverage the ADMM in [30] to more efficiently solve $\mathcal{P}1.1(\bar{\mathbf{v}})$ next.

B. Low-Complexity Design through ADMM

In this subsection, we find the optimal solution to $\mathcal{P}1.1(\bar{\mathbf{v}})$ by the ADMM. More specifically, we first transform $\mathcal{P}1.1(\bar{\mathbf{v}})$ to the following equivalent problem by introducing auxiliary variables $\mathbf{v}_i \in \mathbb{C}^{DN_T}$, $i = 1, 2$.

$$\mathcal{P}1.2(\bar{\mathbf{v}}): \quad \min_{\mathbf{v}, \{\mathbf{v}_i\}} \mathbf{v}^H \mathbf{\Pi} \mathbf{v} \quad (25a)$$

$$\text{s.t.} \quad \mathbf{v} = \mathbf{v}_i, i = 1, 2 \quad (25b)$$

$$\mathbf{v}_1^H \mathbf{v}_1 \leq P_B \quad (25c)$$

$$\mathbf{v}_2^H \bar{\Gamma}_{22}(\bar{\mathbf{v}}) \mathbf{v}_2 - 2\mathcal{R}(\bar{\Gamma}_{12}(\bar{\mathbf{v}}) \mathbf{v}_2) \leq -\bar{\text{MI}}(\bar{\mathbf{v}}). \quad (25d)$$

Let \mathcal{C}_1 and \mathcal{C}_2 denote the feasible regions of (25c) and (25d), respectively. Define the indicator functions as

$$\mathbb{I}_{\mathcal{C}_i}(\mathbf{v}_i) = \begin{cases} 0, & \text{if } \mathbf{v}_i \in \mathcal{C}_i, \\ +\infty, & \text{otherwise} \end{cases}, i = 1, 2. \quad (26)$$

Then, using (26), we can incorporate the constraints (25c) and (25d) into (25a) and construct the following ADMM reformulation of $\mathcal{P}1.1(\bar{\mathbf{v}})$

$$\begin{aligned} \mathcal{P}1.3(\bar{\mathbf{v}}): \quad & \min_{\mathbf{v}, \{\mathbf{v}_i\}} \mathbf{v}^H \mathbf{\Pi} \mathbf{v} + \sum_{i=1}^2 \mathbb{I}_{\mathcal{C}_i}(\mathbf{v}_i) \\ \text{s.t.} \quad & (25b). \end{aligned} \quad (27)$$

The augmented Lagrangian of $\mathcal{P}1.3(\bar{\mathbf{v}})$ is given by

$$\begin{aligned} \mathcal{L}(\mathbf{v}, \{\mathbf{v}_i\}, \{\mathbf{d}_i\}) \\ = \mathbf{v}^H \mathbf{\Pi} \mathbf{v} + \sum_{i=1}^2 \mathbb{I}_{C_i}(\mathbf{v}_i) + \frac{\bar{\rho}}{2} \sum_{i=1}^2 \|\mathbf{v}_i - \mathbf{v} + \mathbf{d}_i\|^2, \end{aligned} \quad (28)$$

where \mathbf{d}_i is the scaled dual variable associated with the constraint $\mathbf{v} = \mathbf{v}_i$, and $\bar{\rho} \geq 0$ denotes the penalty parameter. We can observe that $\mathcal{L}(\mathbf{v}, \{\mathbf{v}_i\}, \{\mathbf{d}_i\})$ can be minimized by updating $\{\mathbf{v}_i\}$ and \mathbf{v} , alternatively. The detailed steps are listed as follows.

1) \mathbf{v}_1 update: The optimization problem w.r.t. \mathbf{v}_1 can be expressed as

$$\begin{aligned} \min_{\mathbf{v}_1} \|\mathbf{v}_1 - (\mathbf{v} - \mathbf{d}_1)\|_2 \\ \text{s.t.} \quad (25c). \end{aligned} \quad (29)$$

Its closed-form solution is given by

$$\mathbf{v}_1 = \min \left\{ \frac{\sqrt{P_B}}{\|\mathbf{v} - \mathbf{d}_1\|_2}, 1 \right\} (\mathbf{v} - \mathbf{d}_1). \quad (30)$$

2) \mathbf{v}_2 update: The optimization problem w.r.t. \mathbf{v}_2 can be expressed as

$$\begin{aligned} \min_{\mathbf{v}_2} \|\mathbf{v}_2 - (\mathbf{v} - \mathbf{d}_2)\|^2 \\ \text{s.t.} \quad (25d). \end{aligned} \quad (31)$$

Using eigen-decomposition, $\bar{\mathbf{\Gamma}}_{22}(\bar{\mathbf{v}})$ becomes $\bar{\mathbf{\Gamma}}_{22}(\bar{\mathbf{v}}) = \mathbf{Q} \tilde{\mathbf{\Lambda}} \mathbf{Q}^H$. Define $\tilde{\mathbf{v}}_2 = \mathbf{Q}^H \mathbf{v}_2$, $\tilde{\mathbf{t}} = \mathbf{Q}^H (\mathbf{v} - \mathbf{d}_2)$ and $\tilde{\mathbf{\Gamma}}_{12}(\bar{\mathbf{v}}) = \bar{\mathbf{\Gamma}}_{12}(\bar{\mathbf{v}}) \mathbf{Q}$. Then, we can rewrite problem (31) as

$$\min_{\tilde{\mathbf{v}}_2} \|\tilde{\mathbf{v}}_2 - \tilde{\mathbf{t}}\|^2 \quad (32a)$$

$$\text{s.t.} \quad \tilde{\mathbf{v}}_2^H \tilde{\mathbf{\Lambda}} \tilde{\mathbf{v}}_2 - 2\mathcal{R}(\tilde{\mathbf{\Gamma}}_{12}(\bar{\mathbf{v}}) \tilde{\mathbf{v}}_2) \leq -\bar{\mathbf{M}}\bar{\mathbf{I}}(\bar{\mathbf{v}}). \quad (32b)$$

Setting the gradient of the Lagrangian of problem (32) to zero, we derive the optimal solution as

$$\tilde{\mathbf{v}}_2 = (\mathbf{I}_{DN_T D} + \tilde{\lambda} \tilde{\mathbf{\Lambda}})^{-1} (\tilde{\mathbf{t}} + \tilde{\lambda} (\tilde{\mathbf{\Gamma}}_{12}(\bar{\mathbf{v}}))^H), \quad (33)$$

where $\tilde{\lambda} \geq 0$ denotes the Lagrange multiplier. If $\tilde{\mathbf{t}}$ satisfies the constraint (32b), we have $\tilde{\lambda} = 0$ and $\tilde{\mathbf{t}}$ is the optimal solution. Otherwise, we have $\tilde{\lambda} > 0$ and the constraint (32b) is satisfied with equality at the optimality of problem (32). To find the optimal $\tilde{\lambda}$, we substitute (33) into the equality constraint $\tilde{\mathbf{v}}_2^H \tilde{\mathbf{\Lambda}} \tilde{\mathbf{v}}_2 - 2\mathcal{R}(\tilde{\mathbf{\Gamma}}_{12}(\bar{\mathbf{v}}) \tilde{\mathbf{v}}_2) = -\bar{\mathbf{M}}\bar{\mathbf{I}}(\bar{\mathbf{v}})$ and obtain the following equation

$$\begin{aligned} f(\tilde{\lambda}) = \sum_{k=1}^{DN_T} \tilde{\mu}_k \left| \frac{\tilde{t}_k + \tilde{\lambda} \tilde{\kappa}_{12}^k}{1 + \tilde{\lambda} \tilde{\mu}_k} \right|^2 \\ - 2\mathcal{R} \left\{ \sum_{k=1}^{DN_T} (\tilde{\kappa}_{12}^k)^* \frac{\tilde{t}_k + \tilde{\lambda} \tilde{\kappa}_{12}^k}{1 + \tilde{\lambda} \tilde{\mu}_k} \right\} + \bar{\mathbf{M}}\bar{\mathbf{I}}(\bar{\mathbf{v}}) = 0, \end{aligned} \quad (34)$$

where \tilde{t}_k and $\tilde{\kappa}_{12}^k$ are the k -th element of vectors $\tilde{\mathbf{t}}$ and $(\tilde{\mathbf{\Gamma}}_{12}(\bar{\mathbf{v}}))^H$, respectively; and $\{\tilde{\mu}_k\}$ denote the eigenvalues of $\bar{\mathbf{\Gamma}}_{22}(\bar{\mathbf{v}})$. Since $f(\tilde{\lambda})$ decreases monotonically, the solution of $f(\tilde{\lambda}) = 0$ is unique. Then, the optimal $\tilde{\lambda}$ can be obtained using the bisection search. After finding $\tilde{\lambda}$, the optimal \mathbf{v}_2 can be calculated as

$$\mathbf{v}_2 = \mathbf{Q} \tilde{\mathbf{v}}_2. \quad (35)$$

Algorithm 1 SCA-ADMM for Solving $\mathcal{P}1$.

Initialization: Initialize $\bar{\mathbf{v}} = \text{vec}(\bar{\mathbf{V}})$ with $\bar{\mathbf{V}}$ being the result of the previous outer iteration. Set the parameter $\bar{\rho}$ and calculate the inverse of the matrix $\mathbf{\Pi} + \bar{\rho} \mathbf{I}_{DN_T}$.

Repeat [SCA Step]

Update $\bar{\mathbf{\Gamma}}_{22}(\bar{\mathbf{v}})$, $\bar{\mathbf{\Gamma}}_{12}(\bar{\mathbf{v}})$ and $\bar{\mathbf{M}}\bar{\mathbf{I}}(\bar{\mathbf{v}})$.

Perform eigen-decomposition on $\bar{\mathbf{\Gamma}}_{22}(\bar{\mathbf{v}})$.

Initialize $\mathbf{d}_i \leftarrow \mathbf{0}, \forall i$ and $\mathbf{v} = \bar{\mathbf{v}}$.

Repeat [ADMM Step]

Update \mathbf{v}_1 and \mathbf{v}_2 according to (30) and (35).

Update \mathbf{v} according to (37).

Update the dual variables $\mathbf{d}_i \leftarrow \mathbf{d}_i + \mathbf{v}_i - \mathbf{v}, i = 1, 2$.

Until ADMM convergence criterion is met.

Update $\bar{\mathbf{v}} = \mathbf{v}$.

Until SCA convergence criterion is met.

3) \mathbf{v} update: The optimization problem w.r.t. \mathbf{v} can be expressed as

$$\min_{\mathbf{v}} \mathbf{v}^H \mathbf{\Pi} \mathbf{v} + \frac{\bar{\rho}}{2} \sum_{i=1}^2 \|\mathbf{v}_i - \mathbf{v} + \mathbf{d}_i\|^2. \quad (36)$$

Setting the gradient of the objective function in (36) to zero, the optimal \mathbf{v} is given by

$$\mathbf{v} = (\mathbf{\Pi} + \bar{\rho} \mathbf{I}_{DN_T})^{-1} \left(\frac{\bar{\rho}}{2} \sum_{i=1}^2 (\mathbf{v}_i + \mathbf{d}_i) \right). \quad (37)$$

Finally, the overall algorithm for solving $\mathcal{P}1$ is summarized in Algorithm 1.

Algorithm 1 is guaranteed to converge to a finite value of $\mathcal{P}1$. Firstly, the ADMM to the convex problem $\mathcal{P}1.1(\bar{\mathbf{v}})$ is convergent [31]. Secondly, the iterative optimization of $\mathcal{P}1.1(\bar{\mathbf{v}})$ in the SCA procedure is non-increasing and the objective function $r(\mathbf{V})$ is lower bounded by 0.

Remark 1 (Complexity Analysis for Algorithm 1): The first computation complexity comes from performing the eigen-decomposition on $\bar{\mathbf{\Gamma}}_{22}(\bar{\mathbf{v}})$ with a complexity of $\mathcal{O}((DN_T)^3)$, which can be done before the ADMM. The second computation complexity comes from performing the matrix inverse on $\mathbf{\Pi} + \bar{\rho} \mathbf{I}_{DN_T}$ with a complexity of $\mathcal{O}((DN_T)^3)$, which can be done before the SCA procedure. The third computation complexity comes from performing the matrix-vector multiplication with a complexity of $\mathcal{O}((DN_T)^2)$ when updating \mathbf{v}_2 and \mathbf{v} . Denote N_{a1} as the number of iteration for the ADMM. Then, the total computational complexity of Algorithm 1 is $\mathcal{O}((N_{s1} + 1)(DN_T)^3 + 2N_{s1}N_{a1}(DN_T)^2)$, which is much less than that of the interior-point methods.

IV. RADAR WAVEFORM DESIGN

In this section, we optimize the radar waveform \mathbf{s} with fixed communication precoder \mathbf{V} , that is,

$$\begin{aligned} \mathcal{P}2: \max_{\mathbf{s}} \sum_{j=0}^J \sigma_{\alpha, j}^2 \frac{\mathbf{s}^H \mathbf{H}_j^H \mathbf{w} \mathbf{w}^H \mathbf{H}_j \mathbf{s}}{\mathbf{s}^H \tilde{\mathbf{R}} \mathbf{s} + r(\mathbf{V})} \\ \text{s.t.} \quad (16a), (16c). \end{aligned}$$

$\mathcal{P}2$ is hard to tackle due to the non-convex constraint (16a) and non-concave fractional objective function. An effective waveform design algorithm will be developed using the SCA and ADMM. We also consider a traditional multi-path suppression scenario for comparison, where the radar detects the target along the direct path and the indirect path returns are regarded as clutter [32]–[34]. This leads to the following waveform design problem⁴.

$$\begin{aligned} \mathcal{Q}2: \max_{\mathbf{s}} & \frac{\mathbf{s}^H \mathbf{H}_0^H \mathbf{w} \mathbf{w}^H \mathbf{H}_0 \mathbf{s}}{\mathbf{s}^H \tilde{\mathbf{R}} \mathbf{s} + r(\mathbf{V})} \\ \text{s.t.} & (16a), (16c), \end{aligned}$$

where $\tilde{\mathbf{R}} = \tilde{\mathbf{R}} + \sum_{j=1}^J \mathbf{H}_j^H \mathbf{w} \mathbf{w}^H \mathbf{H}_j$. The non-convexity of $\mathcal{Q}2$ only comes from the constraint (16a), and the non-concave objective function can be equivalently converted to a quasi-concave one, as shown later. An effective solution is obtained with the SCA and semidefinite programming (SDP) methods. Furthermore, considering the application scene and the hardware limitation, we also study the radar waveform design under some common waveform constraints (e.g., the similarity, per-antenna power and PAPR constraints).

A. Solution to $\mathcal{P}2$ Combining Multi-Path Returns

We first introduce the following lemma to tackle the non-convexity of (16a).

Lemma 4 (SCA-Based Transformation of Constraint (16a)): (16a) is non-convex w.r.t. \mathbf{s} and can be successively approximated by the following convex quadratic constraint

$$\mathbf{s}^H \hat{\Gamma}(\tilde{\mathbf{S}}) \mathbf{s} \leq \widehat{\text{MI}}(\tilde{\mathbf{S}}), \quad (38)$$

where $\tilde{\mathbf{S}} = \bar{\mathbf{s}} \bar{\mathbf{s}}^H$ with $\bar{\mathbf{s}}$ being the solution in the previous SCA iteration.

Proof: Define $\tilde{\mathbf{S}} = \mathbf{s} \mathbf{s}^H$, $\mathbf{R}_v = \sum_{l=1}^L \sigma_{v,l}^2 \mathbf{G}_l \mathbf{V} \mathbf{V}^H \mathbf{G}_l^H$ and $\mathbf{R}_c^k(\tilde{\mathbf{S}}) = \sigma_c^2 \mathbf{I}_{N_R} + \sum_{i=1}^I \sigma_{\gamma,i}^2 \mathbf{G}_{rc}^i(k) \tilde{\mathbf{S}} (\mathbf{G}_{rc}^i(k))^H$. The function $\text{MI}(\mathbf{s}, \mathbf{V})$ can be rewritten as $\text{MI}(\tilde{\mathbf{S}}) = \frac{1}{K} \sum_{k=1}^{\tilde{K}} \left(\log \left| \mathbf{R}_v + \mathbf{R}_c^k(\tilde{\mathbf{S}}) \right| - \log \left| \mathbf{R}_c^k(\tilde{\mathbf{S}}) \right| \right)$. $\text{MI}(\tilde{\mathbf{S}})$ is convex w.r.t. $\tilde{\mathbf{S}}$ and its first-order condition can be given by

$$\text{MI}(\tilde{\mathbf{S}}) \geq \text{MI}(\tilde{\mathbf{S}}) - \text{tr} \left(\hat{\Gamma}(\tilde{\mathbf{S}}) (\tilde{\mathbf{S}} - \tilde{\mathbf{S}}) \right), \quad (39)$$

where [12]

$$\begin{aligned} \hat{\Gamma}(\tilde{\mathbf{S}}) &= - \left(\frac{\partial \text{MI}(\tilde{\mathbf{S}})}{\partial \tilde{\mathbf{S}}} \right)_{\tilde{\mathbf{S}}=\tilde{\mathbf{S}}}^T = \frac{1}{\tilde{K}} \sum_{k=1}^{\tilde{K}} \left(\sum_{i=1}^I \sigma_{\gamma,i}^2 (\mathbf{G}_{rc}^i(k))^H \right. \\ &\quad \left. \left[(\mathbf{R}_c^k(\tilde{\mathbf{S}}))^{-1} - (\mathbf{R}_v + \mathbf{R}_c^k(\tilde{\mathbf{S}}))^{-1} \right] \mathbf{G}_{rc}^i(k) \right) \end{aligned} \quad (40)$$

is the gradient of $\text{MI}(\tilde{\mathbf{S}})$ at $\tilde{\mathbf{S}}$. Thus, the constraint (16a) can be transformed to

$$\text{MI}(\tilde{\mathbf{S}}) - \text{tr} \left(\hat{\Gamma}(\tilde{\mathbf{S}}) (\tilde{\mathbf{S}} - \tilde{\mathbf{S}}) \right) \geq \text{MI}_0. \quad (41)$$

Define

$$\widehat{\text{MI}}(\tilde{\mathbf{S}}) = \text{MI}(\tilde{\mathbf{S}}) + \text{tr} \left(\hat{\Gamma}(\tilde{\mathbf{S}}) \tilde{\mathbf{S}} \right) - \text{MI}_0. \quad (42)$$

⁴The corresponding communication precoder and the radar receive filter can be obtained by similar methods to that in multi-path combining scenarios.

The constraint (41) is equivalent to (38), which is convex due to the positive semidefinite matrix $\hat{\Gamma}(\tilde{\mathbf{S}})$. ■

Next, we will deal with the non-concavity of the objective function. Various techniques have been proposed for the fractional programming, e.g., the Dinkelbach-Type method in [12], [35] and the Charnes-Cooper transformation in [36]. However, these approaches are developed for single-ratio fractional program with quasi-concave objective functions and do not apply for $\mathcal{P}2$ due to the lack of quasi-concavity of the sum-form fractional programming. We resort to the following lemma to convert the non-concave objective function to a series of convex constraints.

Lemma 5 (SCA-Based Transformation of Objective Function): We first introduce an auxiliary variable $y > 0$ satisfying

$$\sum_{j=0}^J \sigma_{\alpha,j}^2 \frac{\mathbf{s}^H \mathbf{H}_j^H \mathbf{w} \mathbf{w}^H \mathbf{H}_j \mathbf{s}}{\mathbf{s}^H \tilde{\mathbf{R}} \mathbf{s} + r(\mathbf{V})} \geq y. \quad (43)$$

Then, (43) can be successively approximated by the following constraint

$$\mathbf{s}^H \tilde{\mathbf{R}} \mathbf{s} + r(\mathbf{V}) - \mathcal{R} \left(\frac{2\bar{\mathbf{s}}^H \tilde{\Psi} \mathbf{s}}{\bar{y}} \right) + \frac{\bar{\mathbf{s}}^H \tilde{\Psi} \bar{\mathbf{s}}}{\bar{y}^2} y \leq 0, \quad (44)$$

where $\tilde{\Psi} = \sum_{j=0}^J \sigma_{\alpha,j}^2 \mathbf{H}_j^H \mathbf{w} \mathbf{w}^H \mathbf{H}_j$ and $(\bar{\mathbf{s}}, \bar{y})$ denotes the solution of previous SCA iteration.

Proof: We first rewritten (43) as

$$\frac{\mathbf{s}^H \tilde{\Psi} \mathbf{s}}{y} \geq \mathbf{s}^H \tilde{\mathbf{R}} \mathbf{s} + r(\mathbf{V}). \quad (45)$$

The first-order condition for the convex function $\mathbf{s}^H \tilde{\Psi} \mathbf{s}/y$ is given by

$$\frac{\mathbf{s}^H \tilde{\Psi} \mathbf{s}}{y} \geq \mathcal{R} \left(\frac{2\bar{\mathbf{s}}^H \tilde{\Psi} \mathbf{s}}{\bar{y}} \right) - \frac{\bar{\mathbf{s}}^H \tilde{\Psi} \bar{\mathbf{s}}}{\bar{y}^2} y, \quad (46)$$

based on which, the constraint (43) can be approximated by (44) around any given point $(\bar{\mathbf{s}}, \bar{y})$. ■

Combining the above lemmas, we have the following proposition.

Proposition 2 (SCA-Based Transformation of $\mathcal{P}2$): $\mathcal{P}2$ can be approximated by a series of convex QCQP problems, i.e.,

$$\begin{aligned} \mathcal{P}2.1(\bar{\mathbf{s}}, \bar{y}): \min_{\mathbf{s}} & \mathcal{R} \left(\hat{\Psi}(\bar{\mathbf{s}}, \bar{y}) \mathbf{s} \right) + \mathbf{s}^H \hat{\mathbf{R}}(\bar{\mathbf{s}}, \bar{y}) \mathbf{s} + \hat{r}(\bar{\mathbf{s}}, \bar{y}) \\ \text{s.t.} & (16c), (38), \end{aligned} \quad (47)$$

where $\hat{\mathbf{R}}(\bar{\mathbf{s}}, \bar{y}) = \bar{y}^2 \tilde{\mathbf{R}} / \bar{\mathbf{s}}^H \tilde{\Psi} \bar{\mathbf{s}}$, $\hat{\Psi}(\bar{\mathbf{s}}, \bar{y}) = -2\bar{y} \bar{\mathbf{s}}^H \tilde{\Psi} / \bar{\mathbf{s}}^H \tilde{\Psi} \bar{\mathbf{s}}$ and $\hat{r}(\bar{\mathbf{s}}, \bar{y}) = \bar{y}^2 r(\mathbf{V}) / \bar{\mathbf{s}}^H \tilde{\Psi} \bar{\mathbf{s}}$.

Proof: Using Lemma 4, we convert the non-convex constraint (16a) into a convex one. Further, using Lemma 5, the convex problem during each iteration of the SCA procedure can be given by

$$\begin{aligned} \mathcal{P}2.2(\bar{\mathbf{s}}, \bar{y}): \max_{\mathbf{s}, y} & y \\ \text{s.t.} & (16c), (38), (44). \end{aligned}$$

$\mathcal{P}2.2(\bar{\mathbf{s}}, \bar{y})$ is equivalent to $\mathcal{P}2.1(\bar{\mathbf{s}}, \bar{y})$ as they have the same optimal solutions and optimal values. Since $\hat{\mathbf{R}}(\bar{\mathbf{s}}, \bar{y})$ is positive semidefinite, $\mathcal{P}2.1(\bar{\mathbf{s}}, \bar{y})$ is a convex QCQP problem. ■

$\mathcal{P}2.1(\bar{\mathbf{s}}, \bar{y})$ can be solved by ADMM similar to Algorithm 1. We first introduce auxiliary variables $\mathbf{s}_k \in \mathbb{C}^{KM_T}$, $k = 1, 2$ and reformulate $\mathcal{P}2.1(\bar{\mathbf{s}}, \bar{y})$ as

$$\mathcal{P}2.3(\bar{\mathbf{s}}, \bar{y}): \min_{\mathbf{s}} \mathcal{R}(\hat{\Psi}(\bar{\mathbf{s}}, \bar{y}) \mathbf{s}) + \mathbf{s}^H \hat{\mathbf{R}}(\bar{\mathbf{s}}, \bar{y}) \mathbf{s} + \hat{r}(\bar{\mathbf{s}}, \bar{y})$$

$$\text{s.t. } \|\mathbf{s}_1\|^2 \leq P_R \quad (48a)$$

$$\mathbf{s}_2^H \hat{\Gamma}(\bar{\mathbf{S}}) \mathbf{s}_2 \leq \widehat{\text{MI}}(\bar{\mathbf{S}}) \quad (48b)$$

$$\mathbf{s}_k = \mathbf{s}, \quad k = 1, 2. \quad (48c)$$

The detailed steps of updating $\{\mathbf{s}_k\}$ and \mathbf{s} are listed as follows.

1) \mathbf{s}_1 update: The optimization problem w.r.t. \mathbf{s}_1 can be expressed as

$$\begin{aligned} \min_{\mathbf{s}_1} \|\mathbf{s}_1 - (\mathbf{s} - \mathbf{g}_1)\|^2 \\ \text{s.t. } (48a), \end{aligned} \quad (49)$$

where \mathbf{g}_1 is the scaled dual variable. The optimal solution to (49) is given by

$$\mathbf{s}_1 = \min \left\{ \frac{\sqrt{P_R}}{\|\mathbf{s} - \mathbf{g}_1\|_2}, 1 \right\} (\mathbf{s} - \mathbf{g}_1). \quad (50)$$

2) \mathbf{s}_2 update: The optimization problem w.r.t. \mathbf{s}_2 can be expressed as

$$\begin{aligned} \min_{\mathbf{s}_2} \|\mathbf{s}_2 - (\mathbf{s} - \mathbf{g}_2)\|^2 \\ \text{s.t. } (48b), \end{aligned} \quad (51)$$

where \mathbf{g}_2 is the scaled dual variable. The optimal solution to (51) is given by

$$\mathbf{s}_2 = \mathbf{U}(\mathbf{I}_{KM_T} + \lambda \mathbf{\Lambda})^{-1} \mathbf{U}^H (\mathbf{s} - \mathbf{g}_2), \quad (52)$$

where \mathbf{U} and $\mathbf{\Lambda}$ come from the eigen-decomposition on $\hat{\Gamma}(\bar{\mathbf{S}})$ i.e., $\hat{\Gamma}(\bar{\mathbf{S}}) = \mathbf{U} \mathbf{\Lambda} \mathbf{U}^H$, and λ denotes the Lagrange multiplier and can be calculated by the bisection method.

3) \mathbf{s} update: The optimization problem w.r.t. \mathbf{s} can be expressed as

$$\min_{\mathbf{s}} \mathcal{R}(\hat{\Psi}(\bar{\mathbf{s}}, \bar{y}) \mathbf{s}) + \mathbf{s}^H \hat{\mathbf{R}}(\bar{\mathbf{s}}, \bar{y}) \mathbf{s} + \frac{\bar{\rho}}{2} \sum_{k=1}^2 \|\mathbf{s}_k - \mathbf{s} + \mathbf{g}_k\|^2, \quad (53)$$

whose optimal solution is given by

$\mathbf{s} =$

$$\left(\hat{\mathbf{R}}(\bar{\mathbf{s}}, \bar{y}) + \bar{\rho} \mathbf{I}_{KM_T} \right)^{-1} \left(\frac{\bar{\rho}}{2} \sum_{k=1}^2 (\mathbf{s}_k + \mathbf{g}_k) - \frac{1}{2} (\hat{\Psi}(\bar{\mathbf{s}}, \bar{y}))^H \right). \quad (54)$$

The overall algorithm for solving $\mathcal{P}2$ is summarized in Algorithm 2.

We can guarantee the convergence of Algorithm 2. Firstly, y is upper-bounded, i.e.,

$$y \leq \sum_{j=0}^J \sigma_{\alpha, j}^2 \frac{\mathbf{s}^H \mathbf{H}_j^H \mathbf{w} \mathbf{w}^H \mathbf{H}_j \mathbf{s}}{\mathbf{s}^H \tilde{\mathbf{R}} \mathbf{s} + r(\mathbf{V})} \leq \frac{\mathbf{s}^H \tilde{\Psi} \mathbf{s}}{r(\mathbf{V})} \leq \hat{\mu} \frac{P_R}{r(\mathbf{V})},$$

where $\hat{\mu}$ denotes the maximum eigenvalue of $\tilde{\Psi}$. Secondly, the iterative optimization of $\mathcal{P}2.1(\bar{\mathbf{s}}, \bar{y})$ is non-decreasing. Thus, the proposed algorithms can converge to a finite value.

Remark 2 (Complexity Analysis for Algorithm 2): The computation complexity mainly comes from calculating the

Algorithm 2 SCA-ADMM for Solving $\mathcal{P}2$.

Initialization: Initialize $\bar{y} = \bar{\mathbf{s}}^H \tilde{\Psi} \bar{\mathbf{s}} / (\bar{\mathbf{s}}^H \tilde{\mathbf{R}} \bar{\mathbf{s}} + r(\mathbf{V}))$ with $\bar{\mathbf{s}}$ being the solution of the previous outer iteration. Set the parameter $\bar{\rho}$.

Repeat [SCA Step]

Update $\hat{\mathbf{R}}(\bar{\mathbf{s}}, \bar{y})$, $\hat{\Psi}(\bar{\mathbf{s}}, \bar{y})$, $\hat{r}(\bar{\mathbf{s}}, \bar{y})$, $\hat{\Gamma}(\bar{\mathbf{S}})$ and $\widehat{\text{MI}}(\bar{\mathbf{S}})$.

Calculate the inverse of the matrix $\hat{\mathbf{R}}(\bar{\mathbf{s}}, \bar{y}) + \bar{\rho} \mathbf{I}_{KM_T}$.

Perform eigen-decomposition on $\hat{\Gamma}(\bar{\mathbf{S}})$.

Initialize $\mathbf{g}_k \leftarrow \mathbf{0}, \forall k$ and $\mathbf{s} = \bar{\mathbf{s}}$.

Repeat [ADMM Step]

Update \mathbf{s}_1 and \mathbf{s}_2 according to (50) and (52).

Update \mathbf{s} according to (54).

Update the dual variables $\mathbf{g}_k \leftarrow \mathbf{g}_k + \mathbf{s}_k - \mathbf{s}, k = 1, 2$.

Until ADMM convergence criterion is met.

Calculate $y = \mathcal{R}(\hat{\Psi}(\bar{\mathbf{s}}, \bar{y}) \mathbf{s}) + \mathbf{s}^H \hat{\mathbf{R}}(\bar{\mathbf{s}}, \bar{y}) \mathbf{s} + \hat{r}(\bar{\mathbf{s}}, \bar{y})$.

Update $\bar{\mathbf{s}} = \mathbf{s}$ and $\bar{y} = y$.

Until SCA convergence criterion is met.

inverse of the matrix $\hat{\mathbf{R}}(\bar{\mathbf{s}}, \bar{y}) + \bar{\rho} \mathbf{I}_{KM_T}$, performing the eigen-decomposition on $\hat{\Gamma}(\bar{\mathbf{S}})$, and the matrix-vector multiplication when updating \mathbf{s}_2 and \mathbf{s} . Denote N_{s2} and N_{a2} as the number of iterations of the SCA and ADMM, respectively. Then, similar to Algorithm 1, the total computational complexity of Algorithm 2 is $\mathcal{O}(2N_{s2}(KM_T)^3 + 2N_{s2}N_{a2}(KM_T)^2)$.

B. Solution to $\mathcal{Q}2$ Suppressing Multi-Path Returns

In this subsection, we focus on solving $\mathcal{Q}2$. Firstly, Lemma 4 is applied to deal with the non-convex constraint (16a), so that $\mathcal{Q}2$ can be successively approximated by

$$\begin{aligned} \mathcal{Q}2.1(\bar{\mathbf{s}}): \max_{\mathbf{s}} \frac{\mathbf{s}^H \mathbf{H}_0^H \mathbf{w} \mathbf{w}^H \mathbf{H}_0 \mathbf{s}}{\mathbf{s}^H \tilde{\mathbf{R}} \mathbf{s} + r(\mathbf{V})} \\ \text{s.t. } (16c), (38). \end{aligned} \quad (55)$$

Then, using the result in [12], the objective function can be equivalently converted to $\mathcal{R}(\mathbf{w}^H \mathbf{H}_0 \mathbf{s}) / \sqrt{\mathbf{s}^H \tilde{\mathbf{R}} \mathbf{s} + r(\mathbf{V})}$, which is a quasi-concave one so that the Dinkelbach-Type iterative algorithm can be applied to obtain the optimal solution to $\mathcal{Q}2.1(\bar{\mathbf{s}})$. However, excessive constraints and tedious iterations will reduce the efficiency of the algorithm. Thus, we develop a non-iterative SDP-based method to achieve the global optimum of $\mathcal{Q}2.1(\bar{\mathbf{s}})$ at a lower cost. The SDP problems that arise at each step of the SCA procedure for solving $\mathcal{Q}2$ are stated in the following proposition.

Proposition 3 (SCA-Based Transformation of $\mathcal{Q}2$): $\mathcal{Q}2$ can be approximated by a series of fractional SDP problems, i.e.,

$$\begin{aligned} \mathcal{Q}2.2(\bar{\mathbf{S}}): \max_{\tilde{\mathbf{S}}} \frac{\text{tr}(\tilde{\Psi} \tilde{\mathbf{S}})}{\text{tr}(\tilde{\mathbf{R}} \tilde{\mathbf{S}}) + r(\mathbf{V})} \\ \text{s.t. } \text{tr}(\tilde{\mathbf{S}}) \leq P_R \\ \text{tr}(\hat{\Gamma}(\bar{\mathbf{S}}) \tilde{\mathbf{S}}) \leq \widehat{\text{MI}}(\bar{\mathbf{S}}) \\ \tilde{\mathbf{S}} \succcurlyeq \mathbf{0}, \text{rank}(\tilde{\mathbf{S}}) = 1, \end{aligned} \quad (56)$$

where $\tilde{\Psi} = \mathbf{H}_0^H \mathbf{w} \mathbf{w}^H \mathbf{H}_0$ with $\text{rank}(\tilde{\Psi}) = 1$.

Proof: Applying the SDP method, $Q2.1(\bar{\mathbf{s}})$ can be equivalently transformed to $Q2.2(\bar{\mathbf{S}})$. A sub-optimal solution to $Q2$ can be obtained by sequentially solving each $Q2.2(\bar{\mathbf{S}})$. ■

$Q2.2(\bar{\mathbf{S}})$ is challenging due to the rank-one constraint. To optimally solve it, we construct the following dual problem

$$Q2.3(\bar{\mathbf{S}}): \min_{\tilde{\mathbf{S}}} \text{tr}(\tilde{\mathbf{S}}) \quad (57a)$$

$$\text{s.t.} \quad \frac{\text{tr}(\tilde{\Psi}\tilde{\mathbf{S}})}{\text{tr}(\tilde{\mathbf{R}}\tilde{\mathbf{S}}) + r(\mathbf{V})} \geq \tilde{p} \quad (57a)$$

$$\text{tr}(\hat{\Gamma}(\bar{\mathbf{S}})\tilde{\mathbf{S}}) \leq \widehat{\text{MI}}(\bar{\mathbf{S}}) \quad (57b)$$

$$\tilde{\mathbf{S}} \succeq \mathbf{0}, \quad (57c)$$

and explore the relationship between the two problems, where \tilde{p} is a non-negative constant. For the SDP problems $Q2.2(\bar{\mathbf{S}})$ and $Q2.3(\bar{\mathbf{S}})$, we have the following result.

Proposition 4 (Optimal Solution of $Q2.2(\bar{\mathbf{S}})$): If \tilde{p} equals to the optimal value of the rank-one semidefinite convex relaxation of $Q2.2(\bar{\mathbf{S}})$, the optimal solution to $Q2.3(\bar{\mathbf{S}})$ is also optimal to $Q2.2(\bar{\mathbf{S}})$.

Proof: See Appendix C. ■

After obtaining the optimal solution $\tilde{\mathbf{S}}_2$ to $Q2.3(\bar{\mathbf{S}})$, we perform eigen-decomposition on it as $\tilde{\mathbf{S}}_2 = \mathbf{s}_2\mathbf{s}_2^H$. Then, \mathbf{s}_2 is optimal to $Q2.1(\bar{\mathbf{s}})$. The overall algorithm for solving $Q2$ is summarized in Algorithm 3.

The convergence analysis of Algorithm 3 is similar to that of Algorithm 2 and we omit it here for brevity.

Remark 3 (Complexity Analysis for Algorithm 3): We can exploit the interior point method to solve the SDP problems $Q2.4(\bar{\mathbf{S}})$ and $Q2.3(\bar{\mathbf{S}})$ with two inequality constraints. Solving each SDP problem requires $\mathcal{O}(\sqrt{2}\log(1/\varepsilon))$ iterations to converge, where ε denotes the relative accuracy and each iteration has a computational complexity of $\mathcal{O}(M_T^{3.5}K^{3.5})$ [28]. Denote N_{s3} as the number of iteration of the SCA method in Algorithm 3. Then, the total computational complexity is $\mathcal{O}(2\sqrt{2}N_{s3}M_T^{3.5}K^{3.5}\log(1/\varepsilon))$.

C. Further Discussion on Practical Waveform Constraints

In this subsection, various constraints are incorporated into $\mathcal{P}2$ and $Q2$ to design adaptive transmit waveforms.

1) *Similarity and Per-Antenna Power Constraints:* The similarity constraint uses a known waveform \mathbf{s}_0 as a benchmark and forces \mathbf{s} to share some good properties of \mathbf{s}_0 in terms of the side-lobe levels and the envelope constancy. Similar to [37], the similarity constraint can be written as

$$\|\mathbf{s} - \zeta\mathbf{s}_0\|^2 \leq \epsilon P_R, \quad |\epsilon|^2 \leq 1, \quad (58)$$

where \mathbf{s}_0 satisfies $\|\mathbf{s}_0\|^2 = P_R$, ϵ determines the level of the similarity and ζ can be used to modulate the power of \mathbf{s}_0 . Using [37], (58) is equivalent to

$$\mathbf{s}^H \left(\mathbf{I}_{KM_T} - \frac{\mathbf{s}_0\mathbf{s}_0^H}{P_R} \right) \mathbf{s} \leq \epsilon P_R. \quad (59)$$

The per-antenna power constraints limit the transmit power at each antenna to a certain threshold, given by [38]

$$\mathbf{s}^H \left(\mathbf{I}_K \otimes \hat{\mathbf{e}}_n \hat{\mathbf{e}}_n^T \right) \mathbf{s} \leq \frac{\rho P_R}{M_T}, \quad n = 1, \dots, M_T, \quad (60)$$

Algorithm 3 SCA-SDP for Solving $Q2$.

Initialization: Initialize $\tilde{\mathbf{S}} = \bar{\mathbf{s}}\bar{\mathbf{s}}^H$ with $\bar{\mathbf{s}}$ being the solution of the previous outer iteration.

Repeat [SCA Step]

Solve $Q2.4(\tilde{\mathbf{S}})$ in (77) to find its optimal value \tilde{p} .

Solve $Q2.3(\tilde{\mathbf{S}})$ in (57) to find its optimal solution $\tilde{\mathbf{S}}_2$.

Update $\tilde{\mathbf{S}} = \tilde{\mathbf{S}}_2$.

Until SCA convergence criterion is met.

Perform eigen-decomposition on $\tilde{\mathbf{S}}_2$ as $\tilde{\mathbf{S}}_2 = \mathbf{s}_2\mathbf{s}_2^H$.

where $\hat{\mathbf{e}}(n) \in \mathbb{C}^{M_T}$ is a direction vector similar to $\mathbf{e}(n)$ and ρ is used to adjust the threshold.

Note that (59) and (60) are all convex quadratic constraints. Therefore, the proposed Algorithm 2 and Algorithm 3 can still be applied to solve $\mathcal{P}2$ and $Q2$ with above constraints, respectively.

2) *PAPR Constraints:* High PAPR values require linear amplifiers with large dynamic range, which is unrealistic in modern radar systems. Thus, we bound the PAPR value at each antenna by the following constraints [39], [40]

$$\|\mathbf{s}\|^2 = P_R \quad (61a)$$

$$\max_{1 \leq n \leq KM_T} \left\{ |s_n|^2 \right\} \leq \frac{\eta P_R}{KM_T}, \quad (61b)$$

where η controls the maximum allowable PAPR value and s_n denotes the n -th element of the waveform \mathbf{s} . In particular, when $\eta = 1$, the PAPR constraint reduces to the constant modulus constraint. Define $\mathbf{F}_n \in \mathbb{C}^{KM_T \times KM_T}$ with the (n, n) -th element being $KM_T/(\eta P_R)$ and other elements being 0. Then, the constraint (61b) can be rewritten as

$$\mathbf{s}^H \mathbf{F}_n \mathbf{s} \leq 1, \quad \forall n = 1, \dots, KM_T. \quad (62)$$

The waveform design problem combining multi-path returns is thus given by

$$\mathcal{P}3: \max_{\mathbf{s}} \sum_{j=0}^J \sigma_{\alpha,j}^2 \frac{\mathbf{s}^H \mathbf{H}_j^H \mathbf{w} \mathbf{w}^H \mathbf{H}_j \mathbf{s}}{\mathbf{s}^H \tilde{\mathbf{R}} \mathbf{s} + r(\mathbf{V})}$$

s.t. (16a), (61a), (62),

which is hard to tackle due to the non-concave objective function and non-convex constraints (16a) and (61a). We can solve $\mathcal{P}3$ by the same SCA procedure in Algorithm 2. During each iteration, we need to solve the following QCQP problem

$$\mathcal{P}3.1(\bar{\mathbf{s}}, \bar{y}): \min_{\mathbf{s}} \mathcal{R}(\hat{\Psi}(\bar{\mathbf{s}}, \bar{y}) \mathbf{s}) + \mathbf{s}^H \hat{\mathbf{R}}(\bar{\mathbf{s}}, \bar{y}) \mathbf{s} + \hat{r}(\bar{\mathbf{s}}, \bar{y})$$

s.t. (38), (61a), (62). (63)

Although $\mathcal{P}3.1(\bar{\mathbf{s}}, \bar{y})$ is non-convex due to the equality constraint (61a), the ADMM performs well and is guaranteed to converge in most cases. If the divergence occurs, we can first solve $\mathcal{P}3.1(\bar{\mathbf{s}}, \bar{y})$ without considering the PAPR constraints (61a) and (62). Then, the obtained solution can be projected onto the feasible sets of (61a) and (62) by adopting the algorithm in [41]. We omit it here for conciseness.

The waveform design problem suppressing multi-path returns can be expressed as

$$\begin{aligned} \mathcal{Q}3: \max_{\mathbf{s}} & \frac{\mathbf{s}^H \mathbf{H}_0^H \mathbf{w} \mathbf{w}^H \mathbf{H}_0 \mathbf{s}}{\mathbf{s}^H \tilde{\mathbf{R}} \mathbf{s} + r(\mathbf{V})} \\ \text{s.t.} & (16\text{a}), (61\text{a}), (62), \end{aligned}$$

which is challenging due to the non-convex constraints (16a) and (61a). We can solve $\mathcal{Q}3$ by the similar SCA method in Algorithm 2. During each iteration, we need to solve the following fractional SDP problem

$$\mathcal{Q}3.1(\tilde{\mathbf{S}}): \max_{\tilde{\mathbf{s}}} \frac{\text{tr}(\tilde{\Psi} \tilde{\mathbf{S}})}{\text{tr}(\tilde{\mathbf{R}} \tilde{\mathbf{S}})} \quad (64\text{a})$$

$$\text{s.t.} \quad \text{tr}(\tilde{\Gamma}(\tilde{\mathbf{S}}) \tilde{\mathbf{S}}) \leq 1 \quad (64\text{b})$$

$$\text{tr}(\tilde{\mathbf{S}}) = P_R \quad (64\text{c})$$

$$\text{tr}(\tilde{\mathbf{F}}_n \tilde{\mathbf{S}}) \leq 1, \forall n \quad (64\text{d})$$

$$\tilde{\mathbf{S}} \succeq \mathbf{0}, \text{rank}(\tilde{\mathbf{S}}) = 1, \quad (64\text{e})$$

where (64a) comes from the original objective function and (61a) with $\tilde{\mathbf{R}} = \tilde{\mathbf{R}} + (r(\mathbf{V})/P_R) \mathbf{I}_{KM_T}$; (64b) comes from (38) and (61a) with $\tilde{\Gamma}(\tilde{\mathbf{S}}) = (\tilde{\Gamma}(\tilde{\mathbf{S}}) + \mathbf{I}_{KM_T})/(\tilde{\mathbf{M}}(\tilde{\mathbf{S}}) + P_R)$; and (64d) comes from (62) and (61a) with $\tilde{\mathbf{F}}_n = (\mathbf{F}_n + \mathbf{I}_{KM_T})/(1 + P_R), \forall n$. It is easy to verify that $\tilde{\mathbf{R}}, \tilde{\Gamma}(\tilde{\mathbf{S}})$ and $\{\tilde{\mathbf{F}}_n\}_{n=1}^{KM_T}$ are all positive definite. The optimal solution to $\mathcal{Q}3.1(\tilde{\mathbf{S}})$ can be find by the following proposition.

Proposition 5 (Optimal Solution of $\mathcal{Q}3.1(\tilde{\mathbf{S}})$): We can solve the rank-one semidefinite convex relaxation of $\mathcal{Q}3.1(\tilde{\mathbf{S}})$ to obtain its optimal solution.

Proof: The optimal solution to $\mathcal{Q}3.1(\tilde{\mathbf{S}})$ after relaxing the rank-one constraint can be calculated based on the Charnes-Cooper transformation [42]. Applying the conclusion in [38, Proposition 2], we can prove that the solution is rank-one. ■

V. NUMERICAL RESULTS AND DISCUSSION

In this section, we will provide numerical examples to evaluate the performances of the proposed algorithms. The number of antennas at the radar transmitter, the radar receiver, the BS and the CU are $M_T = 4$, $M_R = 8$, $N_T = 12$ and $N_R = 3$, respectively. The radar system has the PRI of $\tilde{K} = 100$, the pulse duration of $K = 5$ and maximum transmit power of $P_R = 10$ wats. The communication system has the number of data streams of $D = 3$ and maximum transmit power of $P_B = 1$ walt. The channel parameter settings in the simulations are provided as follows:

- The target is located at range $\tau_0 = 25$ and angle $\theta_0 = 20^\circ$. There are $J = 2$ scatterers causing indirect path returns, which are located in the range of $\tau_1 = 27$, $\tau_2 = 28$, and in the direction of $\theta_1 = -16^\circ$, $\theta_2 = -30^\circ$, respectively. The signal-to-noise ratio along the direct path, given by $\text{SNR}_{r,d} = P_R \sigma_{\alpha,0}^2 / \sigma_r^2$, is set as 10dB, and that along indirect paths, denoted by $\text{SNR}_{r,id} = P_R \sigma_{\alpha,j}^2 / \sigma_r^2, \forall j$, is set as 8dB.
- There are $Q = 7$ scatterers causing clutter returns with $\tilde{\tau}_q$ and $\tilde{\theta}_q$ randomly chosen in $\{K, \dots, \tilde{K}\}$ and $(-5^\circ, 10^\circ)$, respectively. The clutter-to-noise ratio, denoted by $\text{CNR}_r = P_R \sigma_{\alpha,q}^2 / \sigma_r^2, \forall q$, is set as 30dB.

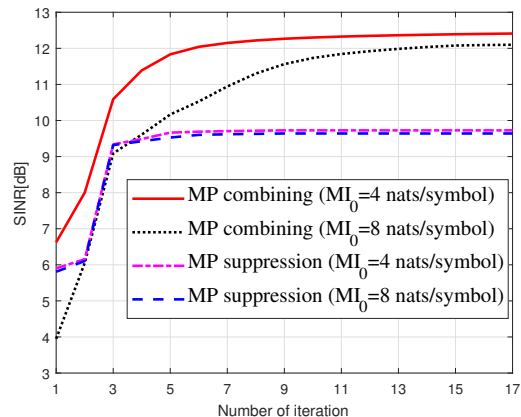


Fig. 2. The radar SINR vs the number of iterations when $\text{MI}_0 = 4, 8$ nats per symbol.

- There are $G = 6$ paths between the BS and the radar receiver with ϕ_{cr}^g and φ_{cr}^g randomly chosen in $(30^\circ, 50^\circ)$ and $(-90^\circ, 90^\circ)$, respectively. The interference-to-noise ratio, denoted by $\text{INR}_r = P_R \sigma_{\beta,g}^2 / \sigma_r^2, \forall g$, is set to 35dB.
- There are $L = 3$ paths between the BS and the CU with ϑ_r^l and ϑ_t^l randomly chosen in $(-90^\circ, 90^\circ)$ and $(-90^\circ, 90^\circ)$, respectively. The signal-to-noise ratio at the CU, denoted by $\text{SNR}_c = P_C \sigma_{v,l}^2 / \sigma_c^2, \forall l$, is set as 25dB.
- There are $I = 6$ paths between the radar and the CU with τ_{rc}^i , φ_{rc}^i and ϕ_{rc}^i randomly chosen in $\{0, \dots, \tilde{K} - 1\}$, $(-90^\circ, 90^\circ)$ and $(25^\circ, 55^\circ)$, respectively. The interference-to-noise ratio at the CU, denoted by $\text{INR}_c = P_C \sigma_{\gamma,i}^2 / \sigma_c^2, \forall i$, is set as 20dB.

In the alternating optimization algorithms, we set $\bar{\rho} = 10$ and $\text{MI}_0 = 6$ [nats per symbol]. The orthogonal linear frequency modulation waveform is chosen as the initial radar waveform, denoted by \mathbf{s}_0 , whose space-time matrix is given by [12], [43]

$$\mathbf{S}_0(m, k) = \frac{e^{j2\pi m(k-1)/M_T} e^{j\pi(k-1)^2/M_T}}{\sqrt{M_T \tilde{K}}},$$

where $m = 1, \dots, M_T$ and $k = 1, \dots, \tilde{K}$. Then, we can obtain $\mathbf{s}_0 = \text{vec}(\mathbf{S}_0)$. The initial communication precoder is given by $\mathbf{V}_0 = \sqrt{P_B/D} [\mathbf{I}_D \mathbf{0}_{D \times (N_T - D)}]^T$. Thus, the initial radar space-time filter can be calculated as $\mathbf{w}_0 = \mathcal{M}(\mathbf{R}^{-1}(\mathbf{V}_0, \mathbf{s}_0) \Psi(\mathbf{s}_0))$. The proposed algorithms terminate when the successive difference of the objective function values is less than 10^{-3} .

We evaluate the convergence performance of the proposed multi-path (MP for short) combining and MP suppression algorithms under different desired communication rate MI_0 in Fig. 2. It can be observed that the radar SINR values in all cases increase continuously during the iteration until the algorithm converges. As expected, exploiting multi-path propagation achieves higher SINR values than suppressing it. This is because the existence of multi-path provides extra information on the target and thus increases the spatial diversity of the radar. Additionally, Fig. 2 clearly shows that relaxing the communication rate constraint will result in a larger SINR

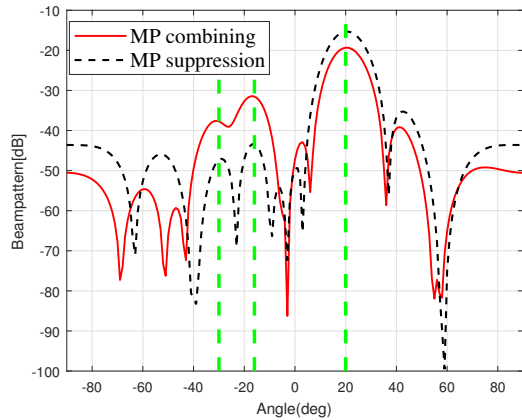
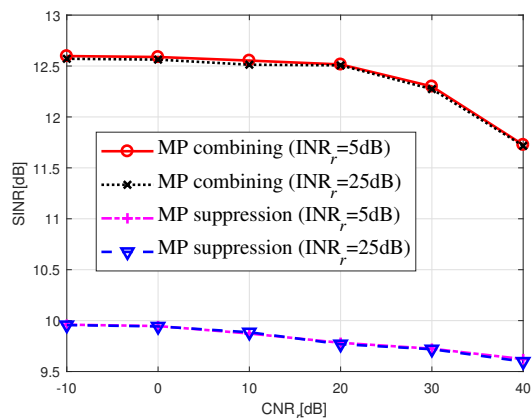


Fig. 3. The radar transceiver beampatterns.

Fig. 4. The radar SINR under different CNR_r and INR_r .

value. This is because a smaller MI_0 will bring larger feasible sets for the optimization problem.

Fig. 3 compares the radar beampatterns of MP combining and MP suppression methods, defined as [44]

$$P(\theta) = \frac{\|\mathbf{w}^H \mathbf{H}_0(\theta) \mathbf{s}\|^2}{M_T M_R \|\mathbf{w}\|^2 \|\mathbf{s}\|^2}.$$

We can observe that the beampattern for the MP combining peaks at the target and multi-path scatterer location. It can also be seen that the beampattern for the MP suppression forms peaks instead of nulls in the directions of multi-path scatterer and the peaks is lower than that of MP combining. This is because multi-path returns carry target information and are suppressed as clutter in the MP suppression method.

In Fig. 4, we investigate the radar SINR performance of MP combining and MP suppression methods under different INR_r and CNR_r . As expected, MP combining method performs better than MP suppression method for the same parameter settings. It is also shown that increasing CNR_r will result in lower SINR values, while increasing INR_r will only marginally degrade the SINR performance. This demonstrates that the proposed algorithm can effectively suppress the mutual interference between systems.

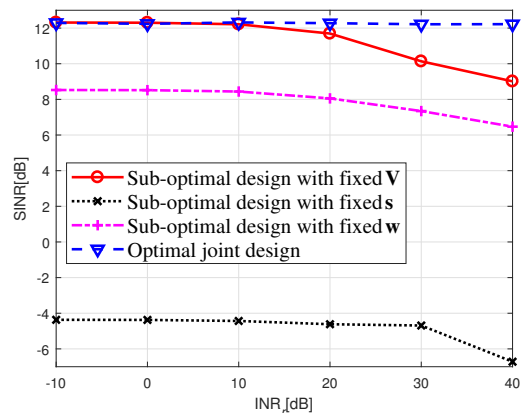
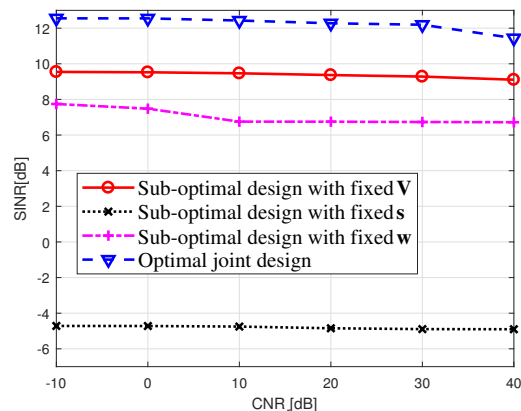
Fig. 5. Comparison with benchmarks under different INR_r .Fig. 6. Comparison with benchmarks under different CNR_r .

Fig. 5 and Fig. 6 compare the radar SINR performance of the MP combining method with the following benchmarks under different INR_r and CNR_r , respectively.

- *Sub-optimal design with fixed V*: We design \mathbf{s} and \mathbf{w} by iteratively solving $\mathcal{P}2$ and updating (8). The communication precoder is fixed as \mathbf{V}_0 .
- *Sub-optimal design with fixed s*: We design \mathbf{V} and \mathbf{w} by iteratively solving $\mathcal{P}1$ and updating (8). The radar waveform is fixed as \mathbf{s}_0 .
- *Sub-optimal design with fixed w*: We design \mathbf{s} and \mathbf{V} by iteratively solving $\mathcal{P}2$ and $\mathcal{P}1$. The radar space-time filter is fixed as \mathbf{w}_0 .

It is shown that the output SINR of the optimal joint design is the highest and can be maintained in a wide range of CNR_r 's and INR_r 's. We can also observe that the performance of the sub-optimal design with fixed \mathbf{V} and the optimal joint design are almost the same when INR_r is low, which indicates that the communication interference can be ignored in this case. The performance gap between these two designs increases with INR_r . This is because, when INR_r is high, the optimal joint design can mitigate the communication interference by allocating the transmit power of the BS to the appropriate direction with the precoder design. As expected, the sub-

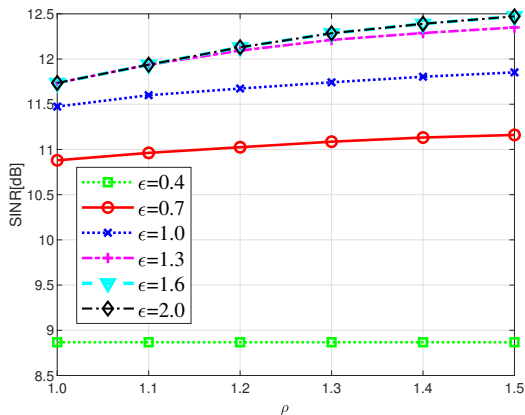


Fig. 7. The radar SINR under different ρ and ϵ .

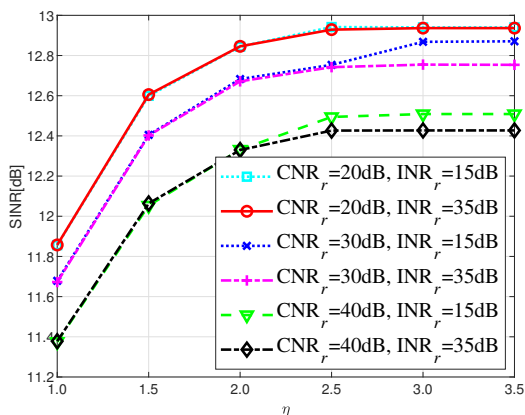


Fig. 8. The radar SINR under different η , INR_r and CNR_r .

optimal design with fixed \mathbf{s} and the sub-optimal design with fixed \mathbf{w} perform poorly, mainly due to the lack of designs for \mathbf{s} and \mathbf{w} , respectively, which is crucial for the radar SINR maximization.

In Fig. 7, we incorporate the similarity and single antenna power constraints into the radar waveform design and study their effects on the radar SINR performance. \mathbf{s}_0 is selected as the reference waveform. We can observe that the SINR increases with ρ and ϵ mainly due to a larger feasible set brought by a larger ρ or ϵ . It can also be noted when ϵ is larger than 1.6, further increasing it will only marginally improve the SINR performance. Moreover, there is no definite improvement of the SINR with increasing ρ when ϵ is small. This is mainly because that the feasible set of the similarity constraint may be contained in that of the single-antenna power constraints.

Finally, Fig 8 investigates the effect of PAPR constraints on the radar SINR performance. As expected, relaxing the PAPR constraints will lead to a larger SINR value. When η is larger than 3.0, further increasing it will not significantly improve the radar SINR. We can also observe that the SINR values degrade with the increase of CNR_r , but can be maintained in a wide range of INR_r 's.

VI. CONCLUSION

In this work, we have considered the coexistence of the pulsed MIMO radar and single-user MIMO communication systems in multi-path environments. The communication precoder, radar transmit waveform and receive filter have been jointly designed to suppress the mutual interference between the two systems while combining the multi-path signals received by each system. The system design has been conducted with the goal of maximizing the radar SINR, while accounting for the constraints on the transmit power of both systems, radar waveform and the transmission rate at the BS. The formulated non-convex problem has been sub-optimally solved by an iterative algorithm based on the alternating maximization, the SCA and ADMM. Simulation results have demonstrated that the proposed algorithm can effectively utilize multi-path signals to achieve better performance and mitigate the interference between the two systems.

APPENDIX A

PROOF OF LEMMA 1

Define $\tilde{\mathbf{a}}_q(\vartheta_r^l, \vartheta_t^l) = \frac{1}{\sqrt{N_R}} e^{-j\pi(q-1)\sin\vartheta_r^l} \mathbf{a}_t(\vartheta_t^l)$, $\Delta_{q_1 q_2}^l = \tilde{\mathbf{a}}_{q_2}^*(\vartheta_r^l, \vartheta_t^l) \tilde{\mathbf{a}}_{q_1}^T(\vartheta_r^l, \vartheta_t^l)$ and

$$\Delta = \sum_{l=1}^L \sigma_{v,l}^2 \begin{bmatrix} \mathbf{I}_D \otimes (\Delta_{11}^l)^T & \cdots & \mathbf{I}_D \otimes (\Delta_{1N_R}^l)^T \\ \vdots & \ddots & \vdots \\ \mathbf{I}_D \otimes (\Delta_{N_R 1}^l)^T & \cdots & \mathbf{I}_D \otimes (\Delta_{N_R N_R}^l)^T \end{bmatrix}. \quad (65)$$

It is easy to verify that the matrix Δ is Hermitian positive semidefinite. Then, the component $\sum_{l=1}^L \sigma_{v,l}^2 \mathbf{G}_l \mathbf{V} \mathbf{V}^H \mathbf{G}_l^H$ in $\text{MI}(\mathbf{s}, \mathbf{V})$ can be reformulated as (66), as shown at the top of next page. Subsequently, the function $\text{MI}_k(\mathbf{s}, \mathbf{V})$ defined in (14) can be rewritten as

$$\begin{aligned} \text{MI}_k(\mathbf{v}) &= \log \left| (\mathbf{I}_{N_R} \otimes \mathbf{v}^T) \Delta (\mathbf{I}_{N_R} \otimes \mathbf{v}^*) (\mathbf{R}_c^k(\mathbf{s}))^{-1} + \mathbf{I}_{N_R} \right| \\ &\stackrel{(a)}{=} \log \left| \Delta^{\frac{1}{2}} (\mathbf{I}_{N_R} \otimes \mathbf{v}^*) (\mathbf{R}_c^k(\mathbf{s}))^{-1} (\mathbf{I}_{N_R} \otimes \mathbf{v}^T) \Delta^{\frac{1}{2}} + \mathbf{I}_{N_R N_T D} \right| \\ &\stackrel{(b)}{=} \log \left| \mathbf{C}(\mathbf{E}_k(\mathbf{v}))^{-1} \mathbf{C}^H \right|, \end{aligned} \quad (67)$$

where the procedure (a) is due to $|\mathbf{I} + \mathbf{A}_1 \mathbf{A}_2| = |\mathbf{I} + \mathbf{A}_2 \mathbf{A}_1|$, the procedure (b) uses the inversion lemma of a partitioned matrix, and the matrix $\mathbf{E}_k(\mathbf{v})$ is given by (19) [45]. Thus, the function $\text{MI}(\mathbf{v}) = \frac{1}{K} \sum_{k=1}^K \text{MI}_k(\mathbf{v})$ is equivalent to $\text{MI}(\mathbf{s}, \mathbf{V})$.

APPENDIX B

PROOF OF LEMMA 2

Since the function $\log \left| \mathbf{C}(\mathbf{E}_k(\mathbf{v}))^{-1} \mathbf{C}^H \right|$ in Lemma 1 is convex w.r.t. $\mathbf{E}_k(\mathbf{v})$ [27], we have the following first-order condition

$$\begin{aligned} \log \left| \mathbf{C}(\mathbf{E}_k(\mathbf{v}))^{-1} \mathbf{C}^H \right| &\geq \log \left| \mathbf{C}(\mathbf{E}_k(\bar{\mathbf{v}}))^{-1} \mathbf{C}^H \right| \\ &\quad + \text{tr}(\mathbf{\Gamma}_k(\bar{\mathbf{v}}) (\mathbf{E}_k(\mathbf{v}) - \mathbf{E}_k(\bar{\mathbf{v}}))), \end{aligned} \quad (68)$$

where

$$\mathbf{\Gamma}_k(\bar{\mathbf{v}}) = -(\mathbf{E}_k(\bar{\mathbf{v}}))^{-1} \mathbf{C}^H \left(\mathbf{C}(\mathbf{E}_k(\bar{\mathbf{v}}))^{-1} \mathbf{C}^H \right)^{-1} \mathbf{C}(\mathbf{E}_k(\bar{\mathbf{v}}))^{-1} \quad (69)$$

$$\begin{aligned}
\sum_{l=1}^L \sigma_{v,l}^2 \mathbf{G}_l \mathbf{V} \mathbf{V}^H \mathbf{G}_l^H &= \sum_{l=1}^L \sigma_{v,l}^2 \mathbf{a}_r(\vartheta_r^l) \mathbf{a}_t^T(\vartheta_t^l) \mathbf{V} \mathbf{V}^H (\mathbf{a}_r(\vartheta_r^l) \mathbf{a}_t^T(\vartheta_t^l))^H = \sum_{l=1}^L \sigma_{v,l}^2 \begin{bmatrix} \text{tr}(\mathbf{V} \mathbf{V}^H \Delta_{11}^l) & \cdots & \text{tr}(\mathbf{V} \mathbf{V}^H \Delta_{1N_R}^l) \\ \vdots & \ddots & \vdots \\ \text{tr}(\mathbf{V} \mathbf{V}^H \Delta_{N_R 1}^l) & \cdots & \text{tr}(\mathbf{V} \mathbf{V}^H \Delta_{N_R N_R}^l) \end{bmatrix} \\
&= \sum_{l=1}^L \sigma_{v,l}^2 \begin{bmatrix} \mathbf{v}^T (\mathbf{I}_D \otimes (\Delta_{11}^l)^T) \mathbf{v}^* & \cdots & \mathbf{v}^T (\mathbf{I}_D \otimes (\Delta_{1N_R}^l)^T) \mathbf{v}^* \\ \vdots & \ddots & \vdots \\ \mathbf{v}^T (\mathbf{I}_D \otimes (\Delta_{N_R 1}^l)^T) \mathbf{v}^* & \cdots & \mathbf{v}^T (\mathbf{I}_D \otimes (\Delta_{N_R N_R}^l)^T) \mathbf{v}^* \end{bmatrix} \\
&= \sum_{l=1}^L \sigma_{v,l}^2 (\mathbf{I}_{N_R} \otimes \mathbf{v}^T) \begin{bmatrix} \mathbf{I}_D \otimes (\Delta_{11}^l)^T & \cdots & \mathbf{I}_D \otimes (\Delta_{1N_R}^l)^T \\ \vdots & \ddots & \vdots \\ \mathbf{I}_D \otimes (\Delta_{N_R 1}^l)^T & \cdots & \mathbf{I}_D \otimes (\Delta_{N_R N_R}^l)^T \end{bmatrix} (\mathbf{I}_{N_R} \otimes \mathbf{v}^*) \\
&= (\mathbf{I}_{N_R} \otimes \mathbf{v}^T) \Delta (\mathbf{I}_{N_R} \otimes \mathbf{v}^*)
\end{aligned} \tag{66}$$

is the gradient of $\log |\mathbf{C}(\mathbf{E}_k(\mathbf{v}))^{-1} \mathbf{C}^H|$ at $\mathbf{E}_k(\bar{\mathbf{v}})$. Thus, the constraint (16a) can be converted to

$$\begin{aligned}
\frac{1}{\bar{K}} \sum_{k=1}^{\bar{K}} \left(\log |\mathbf{C}(\mathbf{E}_k(\bar{\mathbf{v}}))^{-1} \mathbf{C}^H| + \text{tr}(\Gamma_k(\bar{\mathbf{v}}) (\mathbf{E}_k(\mathbf{v}) - \mathbf{E}_k(\bar{\mathbf{v}}))) \right) \\
\geq \text{MI}_0.
\end{aligned} \tag{70}$$

Let $\Gamma_k(\bar{\mathbf{v}})$ be partitioned as

$$\Gamma_k(\bar{\mathbf{v}}) = \begin{bmatrix} \Gamma_k^{11}(\bar{\mathbf{v}}) & \Gamma_k^{12}(\bar{\mathbf{v}}) \\ \Gamma_k^{21}(\bar{\mathbf{v}}) & \Gamma_k^{22}(\bar{\mathbf{v}}) \end{bmatrix}.$$

Then, we can obtain that

$$\begin{aligned}
\text{tr}(\Gamma_k(\bar{\mathbf{v}}) \mathbf{E}_k(\mathbf{v})) &= \text{tr}(\Gamma_k^{11}(\bar{\mathbf{v}})) + \text{tr}(\Gamma_k^{22}(\bar{\mathbf{v}}) \mathbf{R}_c^k(\mathbf{s})) \\
&\quad + 2\mathcal{R} \left(\text{tr}(\Gamma_k^{12}(\bar{\mathbf{v}}) (\mathbf{I}_{N_R} \otimes \mathbf{v}^T) \Delta^{\frac{1}{2}}) \right) \\
&\quad + \text{tr}(\Gamma_k^{22}(\bar{\mathbf{v}}) (\mathbf{I}_{N_R} \otimes \mathbf{v}^T) \Delta (\mathbf{I}_{N_R} \otimes \mathbf{v}^*)).
\end{aligned}$$

Thus, the constraint (70) can be rewritten as

$$\begin{aligned}
2\mathcal{R} \left(\text{tr}(\Gamma_{12}(\bar{\mathbf{v}}) (\mathbf{I}_{N_R} \otimes \mathbf{v}^T) \Delta^{\frac{1}{2}}) \right) \\
+ \text{tr}(\Gamma_{22}(\bar{\mathbf{v}}) (\mathbf{I}_{N_R} \otimes \mathbf{v}^T) \Delta (\mathbf{I}_{N_R} \otimes \mathbf{v}^*)) \geq \bar{\text{MI}}(\bar{\mathbf{v}})
\end{aligned} \tag{71}$$

where $\Gamma_{12}(\bar{\mathbf{v}}) = \frac{1}{\bar{K}} \sum_{k=1}^{\bar{K}} \Gamma_k^{12}(\bar{\mathbf{v}})$, $\Gamma_{22}(\bar{\mathbf{v}}) = \frac{1}{\bar{K}} \sum_{k=1}^{\bar{K}} \Gamma_k^{22}(\bar{\mathbf{v}})$ and

$$\begin{aligned}
\bar{\text{MI}}(\bar{\mathbf{v}}) &= \text{MI}_0 - \frac{1}{\bar{K}} \sum_{k=1}^{\bar{K}} \left(\log |\mathbf{C}(\mathbf{E}_k(\bar{\mathbf{v}}))^{-1} \mathbf{C}^H| - \right. \\
&\quad \left. \text{tr}(\Gamma_k(\bar{\mathbf{v}}) \mathbf{E}_k(\bar{\mathbf{v}})) + \text{tr}(\Gamma_k^{11}(\bar{\mathbf{v}})) + \text{tr}(\Gamma_k^{22}(\bar{\mathbf{v}}) \mathbf{R}_c^k(\mathbf{s})) \right).
\end{aligned} \tag{72}$$

By using $\text{tr}(\mathbf{A}_1^T \mathbf{A}_2) = \text{vec}^T(\mathbf{A}_1) \text{vec}(\mathbf{A}_2)$ and $\text{tr}(\mathbf{A}_1 \mathbf{A}_2 \mathbf{A}_3 \mathbf{A}_4) = \text{vec}^T(\mathbf{A}_4) (\mathbf{A}_1 \otimes \mathbf{A}_3^T) \text{vec}(\mathbf{A}_2^T)$, we can convert (71) to

$$\begin{aligned}
\mathbf{v}^H \mathbf{P}^H \left(\Gamma_{22}(\bar{\mathbf{v}}) \otimes \Delta^T \right) \mathbf{P} \mathbf{v} + 2\mathcal{R} \left(\text{vec}^T \left(\Delta^{\frac{1}{2}} \Gamma_{12}(\bar{\mathbf{v}}) \right) \mathbf{P} \mathbf{v} \right) \\
\geq \bar{\text{MI}}(\bar{\mathbf{v}}),
\end{aligned} \tag{73}$$

where $\mathbf{P} = [\mathbf{P}_1, \mathbf{P}_2, \dots, \mathbf{P}_{N_R}]^T$ with $\mathbf{P}_i = \tilde{\mathbf{e}}_i^T \otimes \mathbf{I}_{N_T D}$ denoting a $N_T D \times N_T D N_R$ matrix for $i = 1, 2, \dots, N_R$ and $\tilde{\mathbf{e}}(n) \in \mathbb{C}^{N_R}$ being a direction vector similar to $\mathbf{e}(n)$. As a result, we can successively approximate the original constraint (16a) by

$$\mathbf{v}^H \bar{\Gamma}_{22}(\bar{\mathbf{v}}) \mathbf{v} - 2\mathcal{R}(\bar{\Gamma}_{12}(\bar{\mathbf{v}}) \mathbf{v}) \leq -\bar{\text{MI}}(\bar{\mathbf{v}}), \tag{74}$$

where

$$\bar{\Gamma}_{22}(\bar{\mathbf{v}}) = -\mathbf{P}^H \left(\Gamma_{22}(\bar{\mathbf{v}}) \otimes \Delta^T \right) \mathbf{P} \tag{75}$$

and

$$\bar{\Gamma}_{12}(\bar{\mathbf{v}}) = \text{vec}^T \left(\Delta^{\frac{1}{2}} \Gamma_{12}(\bar{\mathbf{v}}) \right) \mathbf{P}. \tag{76}$$

Since $\mathbf{E}_k(\mathbf{v})$ is positive definite, $\Gamma_k(\bar{\mathbf{v}})$, $\Gamma_k^{22}(\bar{\mathbf{v}})$ and $\Gamma_{22}(\bar{\mathbf{v}})$ are all negative semidefinite. Hence, $\bar{\Gamma}_{22}(\bar{\mathbf{v}})$ is positive semidefinite and the constraint is convex.

APPENDIX C PROOF OF PROPOSITION 4

After relaxing the rank-one constraint, $\mathcal{Q}2.2(\bar{\mathbf{S}})$ can be converted to

$$\begin{aligned}
\mathcal{Q}2.4(\bar{\mathbf{S}}): \max_{\bar{\mathbf{S}}} \frac{\text{tr}(\tilde{\Psi} \bar{\mathbf{S}})}{\text{tr}(\tilde{\mathbf{R}} \bar{\mathbf{S}}) + r(\mathbf{V})} \\
\text{s.t. } \text{tr}(\tilde{\mathbf{S}}) \leq P_R \\
\text{tr}(\hat{\Gamma}(\bar{\mathbf{S}}) \tilde{\mathbf{S}}) \leq \widehat{\text{MI}}(\bar{\mathbf{S}}) \\
\tilde{\mathbf{S}} \succeq \mathbf{0}.
\end{aligned} \tag{77}$$

Let \tilde{p} and $\tilde{\mathbf{S}}_1$ be the optimal value and optimal solution to $\mathcal{Q}2.4(\bar{\mathbf{S}})$, respectively, which can be calculated based on the Charnes-Cooper transformation same as that in [36]. We further solve $\mathcal{Q}2.3(\bar{\mathbf{S}})$ to obtain its optimal value \tilde{q} and optimal solution $\tilde{\mathbf{S}}_2$.

We first prove that $\mathcal{Q}2.3(\bar{\mathbf{S}})$ and $\mathcal{Q}2.4(\bar{\mathbf{S}})$ share the same optimal solutions. Specifically, it is easy to verify that $\tilde{\mathbf{S}}_1$ is a feasible solution to $\mathcal{Q}2.3(\bar{\mathbf{S}})$. Then, we have $\text{tr}(\tilde{\mathbf{S}}_2) \leq \text{tr}(\tilde{\mathbf{S}}_1) \leq P_R$. Thus, $\tilde{\mathbf{S}}_2$ is a feasible solution to $\mathcal{Q}2.4(\bar{\mathbf{S}})$, which implies

that $\text{tr}(\tilde{\Psi}\tilde{\mathbf{S}}_2)/(\text{tr}(\tilde{\mathbf{R}}\tilde{\mathbf{S}}_2) + r(\mathbf{V})) \leq \tilde{p}$. Since $\tilde{\mathbf{S}}_2$ is the optimal solution to $\mathcal{Q}2.3(\tilde{\mathbf{S}})$, we have $\text{tr}(\tilde{\Psi}\tilde{\mathbf{S}}_2)/(\text{tr}(\tilde{\mathbf{R}}\tilde{\mathbf{S}}_2) + r(\mathbf{V})) \geq \tilde{p}$. Hence, $\text{tr}(\tilde{\Psi}\tilde{\mathbf{S}}_2)/(\text{tr}(\tilde{\mathbf{R}}\tilde{\mathbf{S}}_2) + r(\mathbf{V})) = \tilde{p}$ holds, i.e., the optimal solution to $\mathcal{Q}2.3(\tilde{\mathbf{S}})$ is also optimal to $\mathcal{Q}2.4(\tilde{\mathbf{S}})$.

Next, we prove that optimal solution to $\mathcal{Q}2.3(\tilde{\mathbf{S}})$ is rank-one. Specifically, the Lagrangian of $\mathcal{Q}2.3(\tilde{\mathbf{S}})$ can be given by

$$\begin{aligned} \mathcal{L}(\tilde{\mathbf{S}}_2, \{\lambda_k\}_{k=1}^2, \tilde{\mathbf{Y}}) &= \text{tr}(\tilde{\mathbf{S}}_2) + \lambda_1(\tilde{p}\text{tr}(\tilde{\mathbf{R}}\tilde{\mathbf{S}}_2) + \tilde{p}r(\mathbf{V}) \\ &\quad - \text{tr}(\tilde{\Psi}\tilde{\mathbf{S}}_2)) + \lambda_2(\text{tr}(\hat{\Gamma}(\tilde{\mathbf{S}})\tilde{\mathbf{S}}_2) - \widehat{\text{MI}}(\tilde{\mathbf{S}})) - \text{tr}(\tilde{\mathbf{Y}}\tilde{\mathbf{S}}_2) \\ &= \text{tr}(\mathbf{I}_{KM_T} + \lambda_1\tilde{p}\tilde{\mathbf{R}} - \lambda_1\tilde{\Psi} + \lambda_2\hat{\Gamma}(\tilde{\mathbf{S}}) - \tilde{\mathbf{Y}})\tilde{\mathbf{S}}_2 \\ &\quad + \lambda_1\tilde{p}r(\mathbf{V}) - \lambda_2\widehat{\text{MI}}(\tilde{\mathbf{S}}), \end{aligned} \quad (78)$$

where λ_1 , λ_2 and $\tilde{\mathbf{Y}}$ denote the Lagrange multipliers associated with the constraints (57a), (57b) and (57c), respectively. Setting the gradient of $\mathcal{L}(\tilde{\mathbf{S}}_2, \{\lambda_k\}_{k=1}^2, \tilde{\mathbf{Y}})$ to zero, we obtain

$$\mathbf{I}_{KM_T} + \lambda_1\tilde{p}\tilde{\mathbf{R}} - \lambda_1\tilde{\Psi} + \lambda_2\hat{\Gamma}(\tilde{\mathbf{S}}) - \tilde{\mathbf{Y}} = \mathbf{0}. \quad (79)$$

Define $\Xi = \mathbf{I}_{KM_T} + \lambda_1\tilde{p}\tilde{\mathbf{R}} + \lambda_2\hat{\Gamma}(\tilde{\mathbf{S}}) = \tilde{\mathbf{Y}} + \lambda_1\tilde{\Psi}$. We have $\Xi \succ \mathbf{0}$ and $\text{rank}(\Xi) = KM_T$. On the one hand, since $\tilde{\mathbf{S}}_2 \neq \mathbf{0}$ and $\tilde{\mathbf{Y}}\tilde{\mathbf{S}}_2 = \mathbf{0}$, we can easily infer that $\lambda_1 > 0$ and $\text{rank}(\tilde{\mathbf{Y}}) \leq KM_T - 1$. On the other hand, since $\text{rank}(\Xi) = \text{rank}(\lambda_1\tilde{\Psi} + \tilde{\mathbf{Y}}) \leq \text{rank}(\lambda_1\tilde{\Psi}) + \text{rank}(\tilde{\mathbf{Y}}) = 1 + \text{rank}(\tilde{\mathbf{Y}})$, we have $\text{rank}(\tilde{\mathbf{Y}}) \geq KM_T - 1$. Thus, we obtain $\text{rank}(\tilde{\mathbf{Y}}) = KM_T - 1$. Combined with $\tilde{\mathbf{Y}}\tilde{\mathbf{S}}_2 = \mathbf{0}$, it follows that $\text{rank}(\tilde{\mathbf{S}}_2) \leq 1$. Based on $\tilde{\mathbf{S}}_2 \neq \mathbf{0}$, it can be inferred that $\text{rank}(\tilde{\mathbf{S}}_2) = 1$. That is to say, the optimal solution to $\mathcal{Q}2.3(\tilde{\mathbf{S}})$ is also optimal to $\mathcal{Q}2.2(\tilde{\mathbf{S}})$, and $\mathcal{Q}2.4(\tilde{\mathbf{S}})$ shares the same optimal value as that of $\mathcal{Q}2.2(\tilde{\mathbf{S}})$.

REFERENCES

- [1] H. Griffiths, L. Cohen, S. Watts, E. Mokole, C. Baker, M. Wicks, and S. Blunt, "Radar Spectrum Engineering and Management: Technical and Regulatory Issues," *Proc. IEEE*, vol. 103, no. 1, pp. 85–102, Jan. 2015.
- [2] J. Choi, V. Va, N. Gonzalez-Prelcic, R. Daniels, C. R. Bhat, and R. W. Heath, "Millimeter-Wave Vehicular Communication to Support Massive Automotive Sensing," *IEEE Commun. Mag.*, vol. 54, no. 12, pp. 160–167, Dec. 2016.
- [3] N. C. Luong, X. Lu, D. T. Hoang, D. Niyato, and D. I. Kim, "Radio Resource Management in Joint Radar and Communication: A Comprehensive Survey," *IEEE Commun. Surv. Tutorials*, vol. 23, no. 2, pp. 780–814, 2021.
- [4] R. Saruthirathanaworakun, J. M. Peha, and L. M. Correia, "Opportunistic Sharing Between Rotating Radar and Cellular," *IEEE J. Sel. Areas Commun.*, vol. 30, no. 10, pp. 1900–1910, Nov. 2012.
- [5] Z. Geng, H. Deng, and B. Himed, "Adaptive Radar Beamforming for Interference Mitigation in Radar-Wireless Spectrum Sharing," *IEEE Signal Process. Lett.*, vol. 22, no. 4, pp. 484–488, Apr. 2015.
- [6] H. Deng and B. Himed, "Interference Mitigation Processing for Spectrum-Sharing Between Radar and Wireless Communications Systems," *IEEE Trans. Aerosp. Electron. Syst.*, vol. 49, no. 3, pp. 1911–1919, Jul. 2013.
- [7] N. Nartasilpa, A. Salim, D. Tuninetti, and N. Devroye, "Communications System Performance and Design in the Presence of Radar Interference," *IEEE Trans. Commun.*, vol. 66, no. 9, pp. 4170–4185, Sept. 2018.
- [8] L. Zheng, M. Lops, X. Wang, and E. Grossi, "Joint Design of Overlaid Communication Systems and Pulsed Radars," *IEEE Trans. Signal Process.*, vol. 66, no. 1, pp. 139–154, Jan. 2018.
- [9] F. Wang and H. Li, "Power Allocation for Coexisting Multicarrier Radar and Communication Systems in Cluttered Environments," *IEEE Trans. Signal Process.*, vol. 69, pp. 1603–1613, 2021.
- [10] B. Li, A. P. Petropulu, and W. Trappe, "Optimum Co-Design for Spectrum Sharing between Matrix Completion Based MIMO Radars and a MIMO Communication System," *IEEE Trans. Signal Process.*, vol. 64, no. 17, pp. 4562–4575, Sept. 2016.
- [11] E. Grossi, M. Lops, and L. Venturino, "Joint Design of Surveillance Radar and MIMO Communication in Cluttered Environments," *IEEE Trans. Signal Process.*, vol. 68, pp. 1544–1557, 2020.
- [12] J. Qian, M. Lops, L. Zheng, X. Wang, and Z. He, "Joint System Design for Coexistence of MIMO Radar and MIMO Communication," *IEEE Trans. Signal Process.*, vol. 66, no. 13, pp. 3504–3519, 2018.
- [13] J. Qian, L. Venturino, M. Lops, and X. Wang, "Radar and Communication Spectral Coexistence in Range-Dependent Interference," *IEEE Trans. Signal Process.*, vol. 69, pp. 5891–5906, 2021.
- [14] S. Sen and A. Nehorai, "Adaptive OFDM Radar for Target Detection in Multipath Scenarios," *IEEE Trans. Signal Process.*, vol. 59, no. 1, pp. 78–90, Jan. 2011.
- [15] A. Aubry, A. De Maio, G. Foglia, and D. Orlando, "Diffuse Multipath Exploitation for Adaptive Radar Detection," *IEEE Trans. Signal Process.*, vol. 63, no. 5, pp. 1268–1281, Mar. 2015.
- [16] Z. Xu, C. Fan, J. Wang, and X. Huang, "Robust MIMO Radar Waveform-Filter Design for Extended Target Detection in the Presence of Multipath," *arXiv preprint arXiv:2009.13261*, 2020.
- [17] Z. Xu, C. Fan, and X. Huang, "MIMO Radar Waveform Design for Multipath Exploitation," *IEEE Trans. Signal Process.*, vol. 69, pp. 5359–5371, 2021.
- [18] G. Wang, P. Karanjekar, and G. Ascheid, "Beamforming with time-delay compensation for 60 GHz MIMO frequency-selective channels," in *proc. of IEEE Int. Symp. on Personal, Indoor, and Mobile Radio Commun. (PIMRC)*, Aug. 2015, pp. 387–391.
- [19] G. Wang, J. Sun, and G. Ascheid, "Hybrid Beamforming with Time Delay Compensation for Millimeter Wave MIMO Frequency Selective Channels," in *Proc. IEEE 83rd Veh. Technol. Conf. (VTC Spring)*, May 2016, pp. 1–6.
- [20] M. Rihan and L. Huang, "Optimum Co-Design of Spectrum Sharing Between MIMO Radar and MIMO Communication Systems: An Interference Alignment Approach," *IEEE Trans. Veh. Technol.*, vol. 67, no. 12, pp. 11 667–11 680, 2018.
- [21] A. De Maio, S. De Nicola, Y. Huang, S. Zhang, and A. Farina, "Code Design to Optimize Radar Detection Performance Under Accuracy and Similarity Constraints," *IEEE Trans. Signal Process.*, vol. 56, no. 11, pp. 5618–5629, Nov. 2008.
- [22] R. Schmidt, "Multiple emitter location and signal parameter estimation," *IEEE Trans. Antennas Propag.*, vol. 34, no. 3, pp. 276–280, Mar. 1986.
- [23] L. Xu, J. Li, and P. Stoica, "Target detection and parameter estimation for MIMO radar systems," *IEEE Trans. Aerosp. Electron. Syst.*, vol. 44, no. 3, pp. 927–939, Jul. 2008.
- [24] A. Aubry, A. DeMaio, A. Farina, and M. Wicks, "Knowledge-Aided (Potentially Cognitive) Transmit Signal and Receive Filter Design in Signal-Dependent Clutter," *IEEE Trans. Aerosp. Electron. Syst.*, vol. 49, no. 1, pp. 93–117, Jan. 2013.
- [25] M. Filo, A. Hossain, A. R. Biswas, and R. Piesiewicz, "Cognitive pilot channel: Enabler for radio systems coexistence," in *Proc. 2nd IEEE Int. Workshop Cogn. Radio Adv. Spectrum Manag.*, 2009, pp. 17–23.
- [26] H. Jiang, J.-K. Zhang, and K. M. Wong, "Joint DOD and DOA Estimation for Bistatic MIMO Radar in Unknown Correlated Noise," *IEEE Trans. Veh. Technol.*, vol. 64, no. 11, pp. 5113–5125, Nov. 2015.
- [27] M. M. Naghsh, M. Modarres-Hashemi, M. A. Kerahroodi, and E. H. M. Alian, "An Information Theoretic Approach to Robust Constrained Code Design for MIMO Radars," *IEEE Trans. Signal Process.*, vol. 65, no. 14, pp. 3647–3661, Jul. 2017.
- [28] Y. Nesterov and A. Nemirovskii, *Interior-point polynomial algorithms in convex programming*. SIAM, 1994.
- [29] K.-Y. Wang, A. M.-C. So, T.-H. Chang, W.-K. Ma, and C.-Y. Chi, "Outage Constrained Robust Transmit Optimization for Multiuser MISO Downlinks: Tractable Approximations by Conic Optimization," *IEEE Trans. Signal Process.*, vol. 62, no. 21, pp. 5690–5705, Nov. 2014.
- [30] K. Huang and N. D. Sidiropoulos, "Consensus-ADMM for General Quadratically Constrained Quadratic Programming," *IEEE Trans. Signal Process.*, vol. 64, no. 20, pp. 5297–5310, Oct. 2016.
- [31] S. Boyd, N. Parikh, E. Chu, B. Peleato, J. Eckstein *et al.*, "Distributed optimization and statistical learning via the alternating direction method of multipliers," *Found. Trends Mach. Learn.*, vol. 3, no. 1, pp. 1–122, 2011.
- [32] R. Fante and J. Torres, "Cancellation of diffuse jammer multipath by an airborne adaptive radar," *IEEE Trans. Aerosp. Electron. Syst.*, vol. 31, no. 2, pp. 805–820, Apr. 1995.

- [33] V. Mecca, D. Ramakrishnan, and J. Krolik, "MIMO Radar Space-Time Adaptive Processing for Multipath Clutter Mitigation," in *Fourth IEEE Workshop on Sensor Array and Multichannel Processing, 2006.*, 2006, pp. 249–253.
- [34] G. Hickman and J. L. Krolik, "MIMO GMTI radar with multipath clutter suppression," in *2010 IEEE Sensor Array and Multichannel Signal Process. Workshop*, 2010, pp. 65–68.
- [35] A. Aubry, A. De Maio, and M. M. Naghsh, "Optimizing Radar Waveform and Doppler Filter Bank via Generalized Fractional Programming," *IEEE J. Sel. Areas Commun.*, vol. 9, no. 8, pp. 1387–1399, Dec. 2015.
- [36] X. Yu, G. Cui, Y. Fu, S. Lu, and T. Zhang, "Constrained MIMO radar waveform design for beampattern formation," in *2017 IEEE Radar Conference (RadarConf)*, 2017, pp. 1397–1401.
- [37] A. Aubry, V. Carotenuto, and A. D. Maio, "Forcing Multiple Spectral Compatibility Constraints in Radar Waveforms," *IEEE Signal Process. Lett.*, vol. 23, no. 4, pp. 483–487, Apr. 2016.
- [38] Z. Cheng, B. Liao, Z. He, J. Li, and J. Xie, "Joint Design of the Transmit and Receive Beamforming in MIMO Radar Systems," *IEEE Trans. Veh. Technol.*, vol. 68, no. 8, pp. 7919–7930, Aug. 2019.
- [39] A. De Maio, Y. Huang, M. Piezzo, S. Zhang, and A. Farina, "Design of Optimized Radar Codes With a Peak to Average Power Ratio Constraint," *IEEE Trans. Signal Process.*, vol. 59, no. 6, pp. 2683–2697, Jun. 2011.
- [40] Z. Cheng, C. Han, B. Liao, Z. He, and J. Li, "Communication-Aware Waveform Design for MIMO Radar With Good Transmit Beampattern," *IEEE Trans. Signal Process.*, vol. 66, no. 21, pp. 5549–5562, Nov. 2018.
- [41] J. Tropp, I. Dhillon, R. Heath, and T. Strohmer, "Designing structured tight frames via an alternating projection method," *IEEE Trans. Inf. Theory*, vol. 51, no. 1, pp. 188–209, Jan. 2005.
- [42] A. Charnes and W. W. Cooper, "Programming with linear fractional functionals," *Naval Res. Logistics Quart.*, vol. 9, no. 3-4, pp. 181–186, 1962.
- [43] G. Cui, X. Yu, V. Carotenuto, and L. Kong, "Space-Time Transmit Code and Receive Filter Design for Colocated MIMO Radar," *IEEE Trans. Signal Process.*, vol. 65, no. 5, pp. 1116–1129, Mar. 2017.
- [44] W. Zhu and J. Tang, "Robust Design of Transmit Waveform and Receive Filter For Colocated MIMO Radar," *IEEE Signal Process. Lett.*, vol. 22, no. 11, pp. 2112–2116, Nov. 2015.
- [45] R. A. Horn and C. R. Johnson, *Matrix Analysis*. Cambridge university press, 2012.